

1 **A microbial sulfoquinovose monooxygenase pathway enables sulfosugar assimilation**

2

3 Mahima Sharma,<sup>1</sup> James P. Lingford,<sup>2,3</sup> Marija Petricevic,<sup>4,5</sup> Alexander J.D. Snow,<sup>1</sup> Yunyang  
4 Zhang,<sup>4,5</sup> Michael A. Järvå,<sup>2,3</sup> Janice W.-Y. Mui,<sup>4,5</sup> Nichollas E. Scott,<sup>6</sup> Eleanor C. Saunders,<sup>7</sup>  
5 Runyu Mao,<sup>2,3</sup> Ruwan Epa,<sup>4,5</sup> Bruna M. da Silva,<sup>7,8</sup> Douglas E.V. Pires,<sup>7,8</sup> David B. Ascher,<sup>5,7</sup>  
6 Malcolm J. McConville,<sup>7</sup> Gideon J. Davies,<sup>1\*</sup> Spencer J. Williams,<sup>4,5\*</sup> Ethan D. Goddard-  
7 Borger<sup>2,3\*</sup>

8

9

10 <sup>1</sup> York Structural Biology Laboratory, Department of Chemistry, University of York, Heslington,  
11 YO10 5DD, U.K.

12 <sup>2</sup> The Walter and Eliza Hall Institute of Medical Research, Parkville, Victoria 3052, Australia.

13 <sup>3</sup> Department of Medical Biology, University of Melbourne, Parkville, Victoria 3010, Australia.

14 <sup>4</sup> School of Chemistry, University of Melbourne, Parkville, Victoria 3010, Australia.

15 <sup>5</sup> Bio21 Molecular Science and Biotechnology Institute, University of Melbourne, Parkville,  
16 Victoria 3010, Australia

17 <sup>6</sup> Department of Microbiology and Immunology, University of Melbourne at the Peter Doherty  
18 Institute for Infection and Immunity, Parkville, Victoria 3010, Australia.

19 <sup>7</sup> Department of Biochemistry and Pharmacology, Bio21 Molecular Science and Biotechnology  
20 Institute, University of Melbourne, Parkville, Victoria 3010, Australia

21 <sup>8</sup> School of Computing and Information Systems, University of Melbourne, Melbourne, Victoria  
22 3010, Australia

23

24 Keywords: carbohydrate metabolism, sulfur cycle, oxidative desulfurization

25

26 \*Correspondence and requests for materials should be addressed to G.J.D.  
27 ([gideon.davies@york.ac.uk](mailto:gideon.davies@york.ac.uk)), S.J.W. ([sjwill@unimelb.edu.au](mailto:sjwill@unimelb.edu.au)) or E.D.G.-B. [goddard-  
borger.e@wehi.edu.au](mailto:goddard-<br/>28 borger.e@wehi.edu.au).

29

30 **Abstract**

31 Catabolism of sulfoquinovose (SQ, 6-deoxy-6-sulfoglucose), the ubiquitous sulfosugar produced by  
32 photosynthetic organisms, is an important component of the biogeochemical carbon and sulfur cycles.  
33 Here, we describe a new pathway for SQ degradation that involves oxidative desulfurization to  
34 release sulfite and the intact carbon skeleton of the sugar to support the growth of the plant pathogen  
35 *Agrobacterium tumefaciens*. SQ or its glycoside sulfoquinovosyl glycerol (SQGro) are imported into  
36 the cell by an ABC transporter system with an associated SQ binding protein. A sulfoquinovosidase  
37 hydrolyses the SQ glycoside and the liberated SQ is acted on by a flavin mononucleotide-dependent  
38 sulfoquinovose monooxygenase, in concert with an NADH-dependent flavin reductase, to release  
39 sulfite and 6-oxo-glucose. An NADPH-dependent oxidoreductase reduces the 6-oxo-glucose to  
40 glucose, enabling entry into primary metabolic pathways. Structural and biochemical studies provide  
41 detailed insights into the recognition of key metabolites by proteins in this pathway. Bioinformatic  
42 analyses reveal that the sulfoquinovose monooxygenase (smo) pathway is distributed across Alpha-  
43 and Betaproteobacteria and is especially prevalent within the Rhizobiales order. This strategy for SQ  
44 catabolism is distinct from previously described pathways as it enables the complete utilization of all  
45 carbons within SQ by a single organism with concomitant production of inorganic sulfite.

46

## 47 **Introduction**

48 Sulfoquinovose (SQ; 6-deoxy-6-sulfoglucose) is an anionic sulfosugar found in plant and  
49 cyanobacterial sulfolipids, and in S-layer proteins in archaea<sup>1</sup>. It is estimated that SQ holds around  
50 half of all sulfur in the biosphere, with 10 billion tonnes produced each year in Nature, and so its  
51 cycling is a significant component of the biogeochemical sulfur cycle<sup>2</sup>. Microbial communities play  
52 a dominant role in SQ cycling and usually more than one organism is required to completely  
53 assimilate this source of carbon and sulfur. Organisms with a tier 1 pathway, termed sulfoglycolysis,  
54 perform scission of the C3-C4 bond of SQ to give two three-carbon fragments; carbons 1-3 enter  
55 central metabolism, while carbons 4-6 bearing the sulfonate are excreted as  
56 dihydroxypropanesulfonate (DHPS) or sulfolactate (SL). Organisms with a tier 2 pathway are those  
57 that process DHPS and SL to access the remaining three carbon fragment and release inorganic sulfur.  
58 To date, three tier 1 pathways have been described: the sulfoglycolytic Embden-Meyerhof-Parnas  
59 (sulfo-EMP)<sup>3</sup>, Entner-Doudoroff (sulfo-ED)<sup>4,5</sup> and sulfofructose transaldolase (sulfo-SFT)  
60 pathways<sup>6,7</sup>. Tier 2 metabolism has been described for various specialized bacteria that utilize SL or  
61 DHPS and perform ‘biomineralization’ to release inorganic sulfite, which under aerobic conditions  
62 is readily oxidized to sulfate<sup>1</sup>. While many of the steps in the three tier 1 sulfoglycolysis pathways  
63 differ, all three pathways share the presence of a specialized glycoside hydrolase, a  
64 sulfoquinovosidase (SQase), which catalyzes the hydrolysis of SQ glycosides, such as SQGro, to  
65 release SQ<sup>8,9</sup>.

66  
67 While the tier 1 and 2 pathways described to date require two or more organisms to complete the  
68 ‘biomineralization’ of SQ, there is some evidence that this can also be accomplished by a single  
69 organism. Roy and co-workers have reported that an *Agrobacterium* strain from soil can completely  
70 consume SQ, with release of sulfate, although the genetic and biochemical details behind this process  
71 were not investigated<sup>10</sup>. We previously reported that *A. tumefaciens* C58 contains a functional SQase,  
72 with the ability to hydrolyze SQGro<sup>8</sup>. However, analysis of its genome did not reveal any genes  
73 homologous to those expected for known tier 1 sulfoglycolysis pathways.

74  
75 Here, we investigate the ‘biomineralization’ of SQ by *Agrobacterium tumefaciens* (*Agrobacterium*  
76 *fabrum*) strain C58 and show that this organism effects the oxidoreductive desulfurization of SQ to  
77 release inorganic sulfite and glucose, which can feed into primary metabolism. We show that this  
78 pathway involves: a novel SQ/SQGro solute binding protein and associated ATP-binding cassette  
79 (ABC) transporter; an SQase to release SQ from its glycosides; a flavin-dependent SQ  
80 monooxygenase with paired flavin-reductase to effect oxidative desulfurization of SQ to sulfite and  
81 6-oxo-glucose; and a NADPH-dependent oxidoreductase to reduce 6-oxo-glucose to glucose. X-ray

82 structures determined for each of these proteins in complex with relevant metabolites reveal the  
83 molecular basis of substrate binding and catalysis. We go on to show through bioinformatics analyses  
84 that this pathway – the first to enable the complete assimilation of SQ – is distributed across Alpha-  
85 and Betaproteobacteria and is particularly well-represented within the Rhizobiales order.

86

## 87 **Results**

### 88 ***Differential expression of a gene cluster in the presence sulfoquinovose***

89 To determine if *A. tumefaciens* C58 can utilize SQ as a carbon source, we attempted to grow this  
90 organism in M9 minimal media containing SQ as the sole carbon source. *A. tumefaciens* C58  
91 exhibited robust growth in this media and analysis of spent culture supernatant failed to detect DHPS  
92 or SL. Instead, the culture supernatant accumulated sulfate, but with a lag between consumption of  
93 SQ and sulfate release (**Fig. 1a**), as was previously reported by Roy and co-workers for  
94 *Agrobacterium* sp. strain ABR2<sup>10</sup>. Noting that sulfite is generally released from organosulfonate  
95 degradation pathways<sup>1,11</sup>, we analyzed the supernatant for sulfite (SO<sub>3</sub><sup>2-</sup>), and observed that SQ  
96 consumption is coincident with production of sulfite, which slowly undergoes autooxidation to  
97 sulfate. To investigate the metabolism of the carbon skeleton of SQ, we cultured *A. tumefaciens* on  
98 <sup>13</sup>C<sub>6</sub>-SQ<sup>12</sup> and analyzed the culture supernatant using <sup>13</sup>C NMR spectroscopy (**Supplementary Fig.**  
99 **1**). The only significant <sup>13</sup>C-labelled product we could detect was <sup>13</sup>C-bicarbonate, which formed  
100 transiently during exponential phase growth, and the <sup>13</sup>C-labelled bicarbonate signal disappeared at  
101 stationary phase, presumably through exchange with atmospheric CO<sub>2</sub>. *A. tumefaciens* grew on other  
102 sulfoquinovosides, including SQGro and methyl α-sulfoquinovoside (MeSQ), but did not grow on  
103 other alkylsulfonates including DHPS, SL, sulfoacetic acid, taurine, pentanesulfonate, MES, MOPS,  
104 HEPES, PIPES, cysteic acid or methanesulfonic acid (**Supplementary Fig. 2**). Collectively, this data  
105 demonstrates that *A. tumefaciens* effects the complete metabolism of the carbon backbone of SQ with  
106 concomitant release of sulfite.

107  
108 We performed comparative proteomic experiments to identify changes associated with the growth of  
109 *A. tumefaciens* on SQ compared to glucose at mid-log phase (**Fig. 1b**). The largest and most  
110 significant change we observed was an increase in the abundance of proteins encoded by a single  
111 cluster of genes (*Atu3277-Atu3285*) for cells grown on SQ. Proteins encoded by *Atu3283* and *Atu3284*  
112 were not observed; however, they are predicted to be integral membrane proteins that can be difficult  
113 to detect using conventional proteomic workflows<sup>13</sup>. Thus, the gene cluster *Atu3277-Atu3285*, which  
114 was subsequently renamed *smoA-smoI*, appeared to be important for growth on SQ (**Fig. 1c**). While  
115 the protein encoded by *Atu3285* was previously identified as an SQase<sup>8</sup>, the proteins encoded by other  
116 genes in the cluster were not annotated with functions that were consistent with any tier 1 pathway,  
117 suggesting that *A. tumefaciens* uses a different approach for the catabolism of SQ. The automated  
118 annotations ascribed to the respective gene products in the cluster, which included a putative ABC  
119 transporter system, sulfonate monooxygenase, SDR oxidoreductase, flavin reductase and exporters,  
120 enabled development of a hypothetical biochemical pathway that could explain the complete

121 assimilation of SQ by *A. tumefaciens* (**Fig. 1d**). We proceeded to biochemically validate this  
122 hypothesis and gain structural insights into the proteins involved.

123

#### 124 *Atu3282 (smoF) encodes an ABC transporter solute-binding protein that binds SQGro*

125 Within the gene cluster identified through proteomics, *Atu3281 (smoE)*, *Atu3283 (smoG)*, and  
126 *Atu3284 (smoH)* were annotated as an ABC transporter system, with *Atu3282 (smoF)* encoding an  
127 associated periplasmic solute-binding protein. The substrate preferences of solute binding proteins  
128 are useful for assigning functions to their associated ABC transporters<sup>14</sup>. Accordingly, we produced  
129 recombinant SmoF (**Supplementary Fig. 3**) and demonstrated that it binds SQGro with  $K_d = 290$  nM  
130 ( $\Delta H = -11$  kcal mol<sup>-1</sup>,  $\Delta S = -7$  cal mol<sup>-1</sup> deg<sup>-1</sup>) (**Fig. 2a, Supplementary Table 3**). No binding was  
131 observed for the stereochemically-related monosaccharides D-glucose and D-glucuronic acid.

132

133 To delineate how SmoF recognizes its ligand, we used X-ray diffraction methods to obtain a high-  
134 resolution 3D structure of SmoF in its ligand-free apo state and in complex with SQGro (**Fig. 2b,**  
135 **Supplementary Table 4**). Like most ABC transporter solute-binding proteins, SmoF possesses two  
136 globular domains with a similar  $\alpha/\beta$  fold forming a deep cleft lined with aromatic and polar residues  
137 to capture the ligand. Comparisons of the structures for ligand-free SmoF and the SQGro complex  
138 revealed a large conformational change in the protein resulting from inter-domain rotation upon  
139 SQGro binding. The relative movement of domains was assessed using the DynDom server, which  
140 indicated a hinge rotation of 31° about four linker regions connecting the two domains  
141 (**Supplementary Fig. 4**). SQGro is buried deep within the inter-domain cleft and residues from both  
142 domains accommodate this ligand through a network of hydrogen-bonding interactions (**Fig. 2c,d**).  
143 The sulfonate of SQGro, which is the defining feature of this sulfosugar, is accommodated by  
144 hydrogen-bonds to the side-chain of Thr220 (2.6 Å), backbone amides of Gly166 (3 Å) and Ser43  
145 (2.8 Å), and an ordered water molecule that in turn hydrogen-bonds to the sidechain of His13 (3 Å)  
146 and Gln46 (3.2 Å) (**Fig. 2c,d**). These and the other interactions in the SQGro-bound ‘closed’ state  
147 stabilized SmoF substantially, as evidenced by a 15 °C increase in the protein melting temperature  
148 (**Supplementary Fig. 5**).

149

#### 150 *The structural basis of SQGro recognition by the SQase Atu3285 (SmoI)*

151 We previously reported that *Atu3285 (smoI)* encodes an SQase that preferentially hydrolyses 2'*R*-  
152 SQGro, the natural stereoisomer of this glycoside<sup>8</sup>. To understand the molecular basis of the  
153 preference SmoI has for this stereoisomer, we determined the 3D structure of a pseudo-Michaelis  
154 complex: the inactive acid/base mutant SmoI-D455N in complex with 2'*R*-SQGro (**Fig. 2e,f**). SmoI-  
155 D455N•SQGro crystallized with four protomers in the asymmetric unit, each showing unambiguous

156 density of the substrate bound at the active site. As described previously, the overall fold is an ( $\alpha/\beta$ )<sub>8</sub>  
157 barrel appended with small  $\beta$  sheet domain and the sulfonate group is recognized by  
158 Arg283/Trp286/Tyr491 triad<sup>8</sup>. Arg438 and Glu135 make hydrogen-bonding interactions with the  
159 glyceryl aglycone of 2'R-SQGro. Only Arg438 interacts with the C2-hydroxyl group of the glyceryl  
160 aglycone and thus this residue appears to drive selectivity for the 2'R-SQGro stereoisomer.

161  
162 ***Atu3277 (smoA) encodes a flavin mononucleotide (FMN) reductase***

163 SmoA, annotated as a flavin reductase, was recombinantly expressed in *E. coli* and maintained a  
164 yellow color throughout purification, suggesting that it had co-purified with a flavin co-factor. A  
165 sample of this protein was heat-denatured to release the co-factor and the supernatant analyzed by  
166 LC-MS to reveal that FMN was the sole detectable flavin (**Supplementary Fig. 6**). Michaelis-Menten  
167 kinetics were conducted for SmoA with saturating FMN and NADH or NADPH to determine which  
168 of these reductants was preferred by the enzyme. With NADH the kinetic parameters were  $K_M = 35 \pm 5$   
169  $\mu\text{M}$ ,  $k_{\text{cat}} = 14.5 \pm 0.5 \text{ s}^{-1}$  and  $k_{\text{cat}}/K_M = 4.1 \times 10^5 \text{ M}^{-1} \text{ s}^{-1}$ ; while for NADPH saturation was not observed  
170 and  $k_{\text{cat}}/K_M = 6.8 \times 10^2 \text{ M}^{-1} \text{ s}^{-1}$ , indicating that NADH is the preferred cofactor for SmoA (**Fig. 3a**,  
171 **Supplementary Fig. 7**). Owing to difficulties in obtaining structural data for this enzyme, we also  
172 studied a close homologue from *Rhizobium oryzae* (*RoSmoA*, UniProt accession number:  
173 A0A1X7D6Q3), which possesses a syntenic gene cluster to *Atu3277-Atu3285*. Recombinant  
174 *RoSmoA* also co-purified with FMN (**Supplementary Fig. 6**) and utilized the NADH cofactor with  
175  $K_M = 16 \mu\text{M}$ ,  $k_{\text{cat}} = 33 \text{ s}^{-1}$  and  $k_{\text{cat}}/K_M = 2.1 \times 10^6 \text{ M}^{-1} \text{ s}^{-1}$  (**Supplementary Fig. 7**).

176  
177 ***Atu3279 (smoC) encodes an SQ monooxygenase that desulfurizes SQ***

178 SmoC is annotated as an alkanesulfonate monooxygenase, though it possesses only 30% sequence  
179 identity with the well-characterized alkanesulfonate monooxygenase SsuD, from *E. coli*. SsuD  
180 catalyzes the FMNH<sub>2</sub>- and O<sub>2</sub>-dependent oxidation of alkanesulfonates to produce the corresponding  
181 aldehyde and sulfite, with a preference for pentanesulfonate.<sup>15</sup> The mechanism of this and related  
182 enzymes have been intensively studied yet remain enigmatic. The transformation is thought to involve  
183 initial formation of a C4a-peroxy or N5-peroxy flavin species on-enzyme. One mechanism posits that  
184 the terminal peroxide oxygen attacks the sulfonate sulfur of the substrate before undergoing a  
185 rearrangement to effect C-S bond fission and release of the aldehyde and sulfite products  
186 (**Supplementary Fig. 8a**)<sup>16</sup>. An alternative mechanism suggests the peroxide deprotonates C6, which  
187 is then oxidized to an  $\alpha$ -hydroxysulfonate that undergoes elimination to produce sulfite and the  
188 aldehyde<sup>17</sup>. To demonstrate activity for recombinant SmoC (**Supplementary Fig. 3**), we adapted  
189 assays developed for SsuD that use Ellman's reagent to detect sulfite released by the enzyme<sup>18</sup>. Direct  
190 detection of the putative sugar product, 6-oxo-glucose (6-OG), is not trivial as this molecule exists as

191 a complex equilibrium of (hemi)acetals and hydrates that have poor stability. Thus, SmoC was  
192 incubated with SQ in the presence of SmoA, FMN and NADH, which generate FMNH<sub>2</sub> *in situ*, and  
193 the concentration of sulfite determined periodically using Ellman's reagent (**Fig. 3b**). Maximal  
194 substrate conversion was approximately 200 μM, which is commensurate with the solubility of  
195 molecular oxygen in water under standard conditions, with peak activity observed at pH 8.5  
196 (**Supplementary Fig. 8**). No activity was observed when SQ was replaced with other sulfonates,  
197 including SQGro (the precursor to SQ) or HEPES (an unrelated sulfonate) demonstrating that, unlike  
198 the promiscuous SsuD, SmoC has high specificity for SQ. As such, the hydrolysis of SQGro by SmoI  
199 necessarily precedes oxidative desulfurization by SmoC. This observation is further supported by  
200 ITC, where SQ was found to bind SmoC with  $K_d = 3 \mu\text{M}$  in the absence of any flavin-based cofactors,  
201 whereas no binding was detected for SQGro (**Fig. 3c, Supplementary Table 3**). The unique SQ  
202 monooxygenase activity of SmoC defines this pathway: it is the enzyme that effects fission of the C–  
203 S bond in SQ, and so it was chosen as the namesake for this gene cluster and *Atu3277-Atu3285* were  
204 renamed the **SQ MonoOxygenase** cluster (*smoA-I*).

205

206 While we could readily crystallize SmoC, these crystals only diffracted to a maximum resolution of  
207 3.4 Å. The corresponding low-resolution map suggested that SmoC exists as a dimer, which was  
208 confirmed in solution by SEC-MALS (**Supplementary Fig. 9**). To obtain structural information for  
209 an SQ monooxygenase, we turned to the homolog from *R. oryzae* (*RoSmoC*). Recombinant *RoSmoC*  
210 exhibited similar activity and substrate selectivity for SQ to SmoC (**Supplementary Fig. 8**) and  
211 provided crystals that diffracted to 1.9 Å. Importantly, the low-resolution structure of *A. tumefaciens*  
212 SmoC superimposed with the high-resolution *RoSmoC* structures with a peptide backbone rmsd of  
213 0.4 Å across the entire structure, providing confidence that both enzymes shared a common structure  
214 and function (**Supplementary Fig. 10**). Both SQ monooxygenases consist of a core (α/β)<sub>8</sub> TIM barrel  
215 with three additional insertion regions, analogous to monooxygenases from the bacterial luciferase  
216 family. The protomers exist as a homodimer that buries 4697 Å<sup>2</sup> of surface area, amounting to 18%  
217 of total accessible surface area for each protomer (**Fig. 3d**). Pairwise structural analysis using the  
218 DALI server identified close relationships to a putative luciferase-like monooxygenase (3RAO.pdb)  
219 with an rmsd of 2.4 over 314 residues and a Z score of 34.3, a long-chain alkane monooxygenase  
220 LadA (3B9O.pdb, rmsd 2.6/312 residues, Z-score of 31.0), and FMNH<sub>2</sub>-dependent alkanesulfonate  
221 monooxygenase SsuD (1M41.pdb, rmsd 1.8/317 residues, Z-score of 41.2).

222

223 Comparisons of the *RoSmoC* structure with LadA (3B9O.pdb) in complex with FMN (a pseudo co-  
224 factor) enabled identification of the FMN binding site *RoSmoC*: a deep hydrophobic pocket that  
225 accommodates the isoalloxazine ring system and extends out to the protein-solvent interface, which

226 is gated by conserved phosphate-binding residues Tyr136 and Ser189 (**Fig. 3e**)<sup>19</sup>. The close structural  
227 and functional relationship of *RoSmoC* to alkanesulfonate monooxygenase SsuD (1M41.pdb) was  
228 evident from the conservation of a putative sulfonate binding site comprised of the side-chains  
229 Trp206, Arg236, His238, Tyr341 and His343 (**Fig. 3f**).<sup>18,19</sup> Aside from conferring these enzymes with  
230 an ability to bind sulfonates, these conserved active-site residues have been suggested to contribute  
231 to the stabilization of a peroxyflavin intermediate in SsuD<sup>18,19</sup>. Efforts to obtain crystals of a  
232 *RoSmoC*–SQ complex were unsuccessful, limiting further insights into the origin of enzyme  
233 specificity towards SQ over other sulfonates.

234

### 235 *Atu3278 (smoB) encodes an oxidoreductase that converts 6-oxo-glucose to glucose*

236 SmoB is annotated as a short-chain dehydrogenase/reductase (SDR) and we had hypothesized that it  
237 was responsible for reduction of 6-OG to glucose (**Fig. 1d**). Since 6-OG is difficult to study directly,  
238 we tested our hypothesis by looking for SmoB-mediated isotope incorporation into glucose at  
239 equilibrium (**Fig. 4a**). Assuming our hypothesis to be true, and as a consequence of microscopic  
240 reversibility, incubation of SmoB with a nicotinamide co-factor and glucose in H<sub>2</sub><sup>18</sup>O should result  
241 in transient formation of 6-OG, rapid and reversible hydration/dehydration with H<sub>2</sub><sup>18</sup>O to compete-  
242 out <sup>16</sup>O at C6 for <sup>18</sup>O, and reduction to give 6-<sup>18</sup>O-glucose. In parallel to this process, <sup>18</sup>O  
243 incorporation will occur at C1 of glucose through a similar series of hydration/dehydration reactions.  
244 Before proceeding with these experiments, we used ITC to establish which nicotinamide cofactor was  
245 suitable for SmoB: NADPH bound to SmoB with *K<sub>d</sub>* ~2 μM, while no binding was observed for  
246 NADH (**Supplementary Fig. 11, Supplementary Table S3**). Thus, glucose pre-equilibrated in  
247 H<sub>2</sub><sup>18</sup>O was incubated with SmoB and NADP<sup>+</sup> then analyzed by mass spectrometry to reveal the  
248 formation of a product 4 Da greater in mass than glucose, presumably due to the incorporation of two  
249 <sup>18</sup>O atoms into glucose. The crude reaction mixture was subjected to peracetylation (Ac<sub>2</sub>O/pyridine)  
250 then LC-MS analysis to confirm that the +4 Da product co-eluted with authentic D-glucose-  
251 pentaacetate (**Supplementary Fig. 12**). To determine that the <sup>18</sup>O label was being incorporated at C6  
252 of glucose, we used electron-impact GC-MS, which required conversion of the reaction product to  
253 the acyclic pentapropionate aldonitrile (**Supplementary Fig. 13**)<sup>20</sup>. This approach provided  
254 diagnostic C1-C5 and C5-C6 fragment ions. The <sup>18</sup>O-labelled product gave a C5-C6 fragment that  
255 was 2 mass units higher (*m/z* 173 versus 175), whereas the C1-C5 fragment was the same as  
256 unlabelled glucose reference (*m/z* 370), demonstrating that the <sup>18</sup>O is incorporated at C6. Only  
257 enzymatic reactions conducted in the presence of NADP<sup>+</sup> produced product labelled with <sup>18</sup>O at C6:  
258 NAD<sup>+</sup> failed to produce any product, supporting our observations by ITC and defining the cofactor  
259 specificity of SmoB.

260

261 We determined the 3D structure of SmoB using X-ray diffraction methods. This initial structure  
262 revealed that SmoB exists as a compact trimer, however the C-terminal His<sub>6</sub>-tag in this construct  
263 occupied the putative active site of adjoining subunits, making co-crystallization with cofactors  
264 difficult (**Supplementary Fig. 14**). To overcome this issue, SmoB was subcloned into a different  
265 vector and expressed with a cleavable N-terminal purification tag. This protein maintained the same  
266 catalytic activity and SEC-MALS confirmed it remained a trimer in solution (**Supplementary Fig.**  
267 **15**). This SmoB construct was co-crystallized with NADPH and a ternary product complex obtained  
268 by soaking crystals with D-glucose (**Fig. 4b**). These crystals diffracted to a resolution of 1.5 Å and  
269 the resulting model revealed that SmoB is an (α/β)<sub>8</sub> TIM barrel fold with a C-terminal cofactor  
270 binding site. The overall fold has high structural conservation with members of the aldo-keto  
271 reductase (AKR) superfamily. SmoB binds NADPH with the 2'-phosphate oxygens hydrogen-bonded  
272 to Thr284, Arg289 and backbone amide of Asn285 and the adenine ring stacked between Arg289 and  
273 Phe241 at the C-terminus (**Fig. 4c**). NADPH binds in an extended *anti*-conformation and the  
274 nicotinamide ring is located at the base of the substrate binding pocket. Trp232 makes a π-π stacking  
275 interaction with the nicotinamide ring that positions the reactive center (C4) at a distance of 3 Å from  
276 C-6 of glucose, appropriate for hydride transfer (**Fig. 4d**). Within the SmoB•NADP<sup>+</sup>•glucose  
277 complex, glucose interacts with Arg152 (2.9 Å) and Lys120 (3 Å), as well as His151 (2.8 Å) and  
278 Tyr76 (2.7 Å) within the conserved catalytic tetrad His/Tyr/Lys/Asp that is common to the AKR  
279 superfamily (**Fig. 4e**)<sup>21</sup>.

280

### 281 *SMO pathways occur in the Alphaproteobacteria and Betaproteobacteria*

282 To ascertain how widespread this pathway for SQ utilization might be, a Multigene BLAST search  
283 was conducted of the non-redundant protein set of the NCBI for gene clusters that contain  
284 homologous SQases and SQ monooxygenases. This identified many putative *smo* gene clusters across  
285 the *Agrobacterium* and *Rhizobium* genus within the *Rhizobiales* order and evidence of some broader  
286 expansion into the Alphaproteobacteria and Betaproteobacteria classes (**Fig. 5**). Amongst these  
287 putative *smo* gene clusters, some were syntenic while others were substantially rearranged (non-  
288 syntenic) or modified to make use of other (non-ABC) transporter systems. The use of diverse  
289 transport systems is not surprising: a similar phenomenon has been observed for the tier-1 sulfo-ED  
290 pathway<sup>4,5</sup>. Indeed, sulfo-ED gene clusters have been identified in several *Rhizobiales*<sup>4,5</sup>, suggesting  
291 that there has been ample opportunity for genetic exchanges between these pathways during their  
292 evolution.

293

294 **Discussion**

295 This work builds on a 20 year-old observation that an unclassified *Agrobacterium* strain can grow on  
296 SQ and release inorganic sulfur in the process<sup>10</sup>. We have confirmed this observation and provide a  
297 detailed account of the discovery and biochemical/structural characterisation of the first pathway to  
298 facilitate the complete assimilation of SQ and its glycosides within a single organism. We have also  
299 used this information to provide broader context to the discovery by illustrating this pathway's  
300 distribution amongst other microorganisms, predominantly those of the Alphaproteobacteria class.  
301 The pathway features several proteins with hitherto undescribed activities, including: an SQGro-  
302 binding protein; an FMNH<sub>2</sub>- and O<sub>2</sub>-dependent SQ monooxygenase that defines this 'SMO' pathway  
303 by catalyzing scission of the C-S bond in SQ, and an oxidoreductase dedicated to the NADPH-  
304 dependent reduction of 6-OG to glucose. Like all other sulfoglycolytic pathways studied to date, the  
305 SMO pathway also possesses a conserved SQase, which is essential for liberating SQ from its  
306 precursor glycoside SQGro<sup>8,9</sup>.

307  
308 The SMO pathway shares similarities with other sugar-metabolizing pathways in bacteria. For  
309 example, the presence of SmoI (SQase), SmoF (SQGro binding protein) and SmoE/G/H (ABC  
310 transporter) encoded by the *smo* cluster, is analogous to MalP (maltodextrin phosphorylase), MalE  
311 (maltose binding protein) and MalF/G/K (ABC transporter) encoded by the *mal* operon of *E. coli* that  
312 imports and degrades maltose<sup>22</sup>. Meanwhile, SmoC (SQ monooxygenase) and SmoA (flavin  
313 reductase) of the SMO pathway are reminiscent of the SsuD (FMNH<sub>2</sub>-dependent alkylsulfonate  
314 monooxygenase) and SsuE (NADPH-dependent FMN reductase) pair encoded by the *ssu* operon of  
315 *E. coli* that degrades alkanesulfonates<sup>15</sup>. Indeed, it is feasible, perhaps even likely, that the SMO  
316 pathway arose through the recombination of analogous sugar- and sulfonate-metabolising pathways.

317  
318 Through our structural studies, we have identified key residues involved in sulfosugar recognition  
319 and processing, in order to provide greater confidence to bioinformatic analyses of putative *smo* gene  
320 clusters: an approach that has proven valuable for the identification of tier 1 sulfoglycolytic  
321 pathways<sup>8,23,24</sup>. This includes the Thr220-Gly166-Ser43-H<sub>2</sub>O(His13-Gln46) cluster of SmoF for the  
322 recognition of SQGro, the Arg283-Tryp286-H<sub>2</sub>O(Tyr491) triad of SmoI for the recognition of  
323 SQGro; and the Trp206-Arg236-His238-Tyr341-His343 constellation of SmoC for the recognition  
324 of SQ. Given the importance of the SQ monooxygenase SmoC to the SMO pathway, further empirical  
325 and computational work is warranted to understand what interactions drive its selectivity for SQ,  
326 which lies in contrast with the promiscuity exhibited by alkanesulfonate monooxygenases like SsuD.

327

328 The prevalence of the SMO pathway in bacteria of the *Rhizobiales* order is intriguing, since many  
329 members of this order are plant symbionts or pathogens. Indeed, those that do not possess an SMO  
330 pathway often possess a complementary tier 1 sulfo-ED pathway<sup>4</sup>. Accordingly, it appears that plant  
331 sulfolipid catabolism is important for bacteria in this order, whether they be plant  
332 pathogens/symbionts or free-living organisms adopting an oligotrophic saprophytic lifestyle in  
333 substrate replete with decaying plant tissues. Symbiotic bacteria of the *Rhizobiales* order reside within  
334 the root nodules of their plant host, where they harness four-carbon substrates from the host for energy  
335 and central metabolism<sup>25</sup>. Sugawara and co-workers showed that sulfonate utilization gene clusters  
336 were expressed by the plant symbiont *Bradyrhizobium diazoefficiens* USDA 110 within these nodules  
337 and that this may be important for utilizing diverse sulfur sources to support symbiotic and possibly  
338 free-living lifestyles<sup>26</sup>. With sulfolipid representing a large and accessible pool of sulfur in plants,  
339 one possible purpose of the SMO pathway may be to salvage sulfur for these bacteria. This is an  
340 important distinction between the SMO pathway and the tier 1 sulfoglycolytic pathways: the latter  
341 supports two-member microbial communities containing a second member with a tier 2 pathway to  
342 provide access to the sulfur of SQ<sup>27</sup>. In this sense, use of the SMO pathway, which enables the  
343 complete utilization of the carbon skeleton and access to the sulfur of the monosaccharide can be  
344 considered a ‘selfish’ metabolic strategy, and could provide an advantage in the highly competitive  
345 soil environment or in the absence of other bacterial species within colonized plant tissues. These  
346 ideas, combined with the pathway’s requirement for molecular oxygen to effect C–S bond fission,  
347 likely explain why the SMO pathway occurs within those bacteria that are commonly associated with  
348 plants. Understanding how the SMO and tier 1 pathways impact fitness within the different  
349 environmental niches discussed here remains an important question, with answers that have  
350 significant implications for understanding plant diseases and symbioses, as well as soil chemistry.  
351

352 **Methods**

353

354 *Growth studies*

355 Cultures of *A. tumefaciens* C58 were grown in a phosphate-buffered mineral salts media (M9, pH  
356 7.2), with glucose or SQ (10 mM) as the sole carbon source. Cultures were incubated at 30 °C (250  
357 rpm), with adaptation and robust growth observed within 2–3 days. These were sub-cultured (1%  
358 inoculum) into the same media (10 ml) and grown at 30 °C (250 rpm). Bacterial growth was  
359 quantitated using a Varian Cary50 UV/visible spectrophotometer to measure OD<sub>600</sub>. Growth  
360 experiments were replicated twice.

361

362 *Reducing sugar assay for culture supernatant*

363 The reducing sugar assay was performed according to the procedure of Blakeney and Mutton<sup>28</sup>. This  
364 assay uses pre-prepared alkaline diluent and PAHBAH working solution. Alkaline diluent was  
365 prepared by the addition of sodium hydroxide (20 g, 0.50 mol) to a solution of 0.10 M trisodium  
366 citrate (50 mmol, 500 ml) and 0.02 M calcium chloride (13 mmol, 500 ml). PAHBAH working  
367 solution was prepared by dissolving 4-hydroxybenzhydrazide (PAHBAH) (0.25 g, 1.6 mmol) in  
368 alkaline diluent (50 ml). The PAHBAH working solution should be made fresh shortly before use.  
369 To determine reducing sugar concentration, 0.90 ml of PAHBAH working solution was added to 0.10  
370 ml of sample. The mixture was heated at 98 °C for 4 min then 0.5 ml of the mixture was diluted into  
371 1.0 ml of deionized water and the absorbance read at 415 nm using a Varian Cary50 UV/visible  
372 spectrophotometer. Concentrations of SQ were determined with reference to a standard curve  
373 constructed using SQ.

374

375 *Turbidometric sulfate assay for culture supernatant*

376 The sulfate assay was performed according to the procedure of Sörbo<sup>29</sup>. This assay uses a Ba-PEG  
377 reagent, which contains PEG to stabilize BaSO<sub>4</sub> crystals and a small amount of pre-formed BaSO<sub>4</sub>  
378 seed crystals to improve the reproducibility and linearity of the assay. The Ba-PEG reagent should be  
379 prepared fresh before use. Ba-PEG reagent was prepared by dissolving BaCl<sub>2</sub> (42 mg, 0.20 mmol)  
380 and polyethylene glycol 6000 (0.75 g) in deionized water (5.0 ml). A small amount of Na<sub>2</sub>SO<sub>4</sub> (10  
381 µl, 50 mM) was added to this solution, with efficient magnetic stirring to generate preformed BaSO<sub>4</sub>  
382 seed crystals. Individual sulfate assays were conducted as follows. A sample (typically 100 µl,  
383 containing a maximum of 2.5 µmol of Na<sub>2</sub>SO<sub>4</sub>) was diluted to 0.1 ml with deionized water before the  
384 addition of 0.5 M HCl (0.1 ml) followed by Ba-PEG reagent (0.1 ml). The mixture was mixed  
385 vigorously and the absorbance of the sample at 400 nm determined using a Varian Cary50 UV/visible

386 spectrophotometer. Concentrations of sulfate were determined by reference to a standard curve  
387 constructed using Na<sub>2</sub>SO<sub>4</sub>.

388

#### 389 *Colorimetric fuchsin sulfite assay for culture supernatant*

390 The fuchsin sulfite assay was performed according to the procedures of Brychkova *et al.*<sup>30</sup> and  
391 Kurmanbayeva *et al.*<sup>31</sup>. This procedure requires three pre-prepared solutions, Reagents A, B and C.  
392 Reagent A was prepared by dissolution of basic fuchsin (4.0 mg, 12 μmol) in deionized water (8.25  
393 ml) at 0 °C, prior to the addition of 98% H<sub>2</sub>SO<sub>4</sub> (1.25 ml). Reagent B was prepared by diluting  
394 formaldehyde (36% in H<sub>2</sub>O, 0.32 ml) in deionized water (9.68 mL) at 0°C. Reagent C was prepared  
395 by dilution of Reagent A (1 ml) in deionized water (7 ml), prior to the addition of solution reagent B  
396 (1 ml). Individual sulfite assays were performed by addition of Reagent C (516 μl) to a mixture of  
397 sample (72 μl) and 0.5 mM Na<sub>2</sub>SO<sub>3</sub> (12 μl), with the latter providing a stable background signal for  
398 reference. The sample was incubated at r.t. for 10 min and the absorbance of the sample at 570 nm  
399 determined using a Varian Cary50 UV/visible spectrophotometer. Concentrations of sulfite were  
400 determined by reference to a standard curve constructed using Na<sub>2</sub>SO<sub>3</sub>.

401

#### 402 *NMR analysis of metabolites produced from (<sup>13</sup>C<sub>6</sub>)SQ*

403 M9 minimal media (5 ml) containing 10 mM glucose was inoculated with *A. tumefaciens* C58 and  
404 grown to stationary phase at 30 °C (250 rpm). A 50 μl aliquot of this culture was used to inoculate 2  
405 ml of M9 minimal media containing 10 mM (<sup>13</sup>C<sub>6</sub>)SQ and the culture incubated at 30 °C (250 rpm).  
406 At OD<sub>600</sub> 0.27 and OD<sub>600</sub> 0.49, 950 μl samples of culture supernatant were diluted with 100 μl of D<sub>2</sub>O  
407 and <sup>13</sup>C-NMR spectra acquired using a 400 MHz spectrophotomer (100 MHz for <sup>13</sup>C).

408

#### 409 *Growth of A. tumefaciens C58 on diverse alkanesulfonates*

410 M9 minimal media (5 ml) containing 10 mM glucose was inoculated with *A. tumefaciens* C58 and  
411 grown to stationary phase at 30 °C (250 rpm). A 50 μl aliquot of this starter culture was used to  
412 inoculate 2 ml of M9 minimal media containing 10 mM of the alternative alkanesulfonate substrate:  
413 SQ (positive control), methyl α-sulfoquinovoside (MeSQ), glycer-1-yl α-sulfoquinovoside (SQGro),  
414 dicyclohexylammonium sulfolactate, cyclohexylammonium dihydroxypropanesulfonate, sulfoacetic  
415 acid, taurine, sodium pentanesulfonate, cysteic acid, MOPS, HEPES, PIPES, MES and  
416 methanesulfonic acid. Cultures were incubated for 30 days at 30 °C (250 rpm) with daily observations  
417 of optical density at 600 nm. Each experiment was performed in duplicate. Growth was observed on  
418 SQ (positive control), MeSQ, and SQGro, but not on any other sulfonate. Control experiments  
419 established that *A. tumefaciens* grows on glucose in the presence and absence of cyclohexylamine or  
420 dicyclohexylamine, and does not grow on cyclohexylamine or dicyclohexylamine alone.

421

422 *Digestion of samples for quantitative proteomics*

423 Freeze dried *A. tumefaciens* whole-cell pellets were resuspend in 500 µl lysis buffer (4% SDS, 50  
424 mM Tris pH 8.5, 10 mM DTT) and boiled at 95 °C for 10 min with shaking at 2000 rpm to shear  
425 DNA and inactivate protease activity. Lysates were cooled to room temperature and protein  
426 concentration determined using a BCA assay. Each sample (200 µg of protein) was acetone  
427 precipitated by mixing 4 volumes of ice-cold acetone with one volume of sample. Samples were  
428 precipitated overnight at -20 °C and then centrifuged at 4000 × g for 10 min at 4 °C. The precipitated  
429 protein pellets were resuspended with 80% ice-cold acetone and precipitated for an additional 4 h at  
430 -20 °C. Samples were centrifuged at 17000 × g for 10 min at 4 °C to collect precipitated protein, the  
431 supernatant was discarded and excess acetone driven off at 65 °C for 5 min. Dried protein pellets  
432 were resuspended in 6 M urea, 2 M thiourea, 40 mM NH<sub>4</sub>HCO<sub>3</sub> and reduced/alkylated prior to  
433 digestion with Lys-C (1/200 w/w) then trypsin (1/50 w/w) overnight as previously described<sup>32</sup>.  
434 Digested samples were acidified to a final concentration of 0.5% formic acid and desalted using C18  
435 stage tips<sup>33</sup> before analysis by LC-MS.

436

437 *Quantitative proteomics using reversed phase LC-MS*

438 Purified peptides were resuspended in Buffer A\* (2% MeCN, 0.1% TFA) and separated using a  
439 Proflow-equipped Dionex Ultimate 3000 Ultra-Performance Liquid Chromatography system  
440 (Thermo Fisher Scientific) with a two-column chromatography set up composed of a PepMap100  
441 C18 20 mm × 75 µm trap and a PepMap C18 500 mm × 75 µm analytical column (Thermo Fisher  
442 Scientific). Samples were concentrated onto the trap column at 5 µl min<sup>-1</sup> with Buffer A (2% MeCN,  
443 0.1% FA) for 6 min and then infused into an Orbitrap Q-Exactive HF Mass Spectrometer (Thermo  
444 Fisher Scientific) at 250 nl min<sup>-1</sup>. Peptides were separated using 124-min gradients altering the buffer  
445 composition from 2% Buffer B (80% MeCN, 0.1% FA) to 8% B over 14 min, then from 8% B to  
446 30% B over 80 min, 30% B to 45% B over 10 min, 45% B to 95% B over 2 min, holding at 95% B  
447 for 10, then dropped to 2% B over 1 min and holding at 2% B for the remaining 7 min. The Q-  
448 Exactive HF™ Mass Spectrometer was operated in a data-dependent mode automatically switching  
449 between the acquisition of a single Orbitrap MS scan (120,000 resolution) and a maximum of 20 MS-  
450 MS scans (HCD NCE 28, maximum fill time 40 ms, AGC 2×10<sup>5</sup> with a resolution of 15,000).

451

452 *Mass spectrometry data analysis*

453 Proteomics datasets were searched using MaxQuant (v1.5.3.3)<sup>34</sup> against the *A. tumefaciens* C58  
454 proteome (Uniprot proteome id UP000000813, downloaded 27/01/2018, 5344 entries). Searches were  
455 performed with carbamidomethylation of cysteine set as a fixed modification and oxidation of

456 methionine as well as acetylation of protein N-termini allowed as variable modifications. The  
457 protease specificity was set to trypsin allowing 2 miscleavage events with a maximum false discovery  
458 rate (FDR) of 1.0% set for protein and peptide identifications. To enhance the identification of  
459 peptides between samples the Match Between Runs option was enabled with a precursor match  
460 window set to 2 min and an alignment window of 10 min. For label-free quantitation, the MaxLFQ  
461 option within Maxquant<sup>35</sup> was enabled in addition to the re-quantification module. The resulting  
462 protein group output was processed within the Perseus (v1.4.0.6)<sup>36</sup> analysis environment to remove  
463 reverse matches and common protein contaminants prior. For LFQ comparisons missing values were  
464 imputed using Perseus and Pearson correlations visualized using R. The mass spectrometry  
465 proteomics data have been deposited to the ProteomeXchange Consortium via the PRIDE<sup>37</sup> partner  
466 repository with the dataset identifier PXD014115.

467

#### 468 *Cloning*

469 Oligonucleotides encoding *Atu3277* (SmoA), *Atu3278* (SmoB), *Atu3279* (SmoC) and *Atu3282*  
470 (SmoF) were amplified by PCR using Phusion polymerase HF master mix (NEB), the appropriate  
471 primers listed in **Supplementary Table 1** and *A. tumefaciens* C58 gDNA as template.  
472 Oligonucleotides encoding *RoSmoA* and *RoSmoC* were synthesized (IDT) to provide the sequences  
473 listed in **Supplementary Table 1**. These were cloned into the pET29b(+) vector at the *NdeI* and *XhoI*  
474 sites and sequence-verified by Sanger sequencing to give expression vectors for SmoA, SmoB,  
475 SmoC, SmoF, *RoSmoA* and *RoSmoC*. Due to interference from the SmoB C-terminal His<sub>6</sub>-tag during  
476 structural studies, the *smoB* (*Atu3278*) gene was sub-cloned into the pET-YSBLIC3C vector<sup>38</sup> by  
477 PCR amplification with the relevant primers in **Supplementary Table 1** and In-Fusion<sup>®</sup> cloning  
478 (Clontech Laboratories, Inc.) into linearized YSBLIC3C vector according to the manufacturer's  
479 protocol. The expression plasmid was sequence-verified by Sanger sequencing.

480

#### 481 *Protein expression and purification*

482 All vectors were transformed into 'T7 Express' *E. coli* (NEB), except for the vector encoding SmoF  
483 (*Atu3282*), which was transformed into 'Shuffle<sup>®</sup> T7' *E. coli* (NEB), and all were plated onto LB-  
484 agar (50 µg/ml kanamycin) and incubated at 37 °C for 16 h. A single colony was used to inoculate  
485 10 ml of LB media containing 50 µg/ml kanamycin and the cultures incubated at 37 °C for 16 h.  
486 These starter cultures were used to inoculate 1000 ml of S-broth (35 g tryptone, 20 g yeast extract, 5  
487 g NaCl, pH 7.4) containing 50 µg/ml kanamycin, which was incubated with shaking (250 rpm) at 37  
488 °C until it reached an OD<sub>600</sub> of 0.8. Each culture was cooled to room temperature, isopropyl  
489 thiogalactoside (IPTG) added to a final concentration of 400 µM, and incubation with shaking (200  
490 rpm) continued at 18 °C for 19 h. Cells were harvested by centrifugation at 8,000 g for 20 min at 4

491 °C then resuspended in 40 ml binding buffer (50 mM NaPi, 300 mM NaCl, 5 mM imidazole, pH 7.5)  
492 containing protease inhibitor (Roche cOmplete EDTA-free protease inhibitor cocktail) and lysozyme  
493 (0.1 mg/ml) by nutating at 4 °C for 30 min. Benzonase (1 µl) was added to the mixture then lysis was  
494 effected by sonication [10× (15 s on / 45 s off) at 45% amplitude]. The lysate was centrifuged at  
495 18,000 g for 20 min at 4 °C and the supernatant collected. The supernatants were filtered (0.45 µm)  
496 and loaded onto a 1 ml HiTrap TALON IMAC column (GE). The column was washed with 3 × 10  
497 ml of binding buffer, then the protein was eluted using elution buffer (50 mM NaPi, 300 mM NaCl,  
498 400 mM imidazole, pH 7.5). Fractions containing product, as judged by SDS-PAGE, were further  
499 purified by size exclusion chromatography on a HiPrep 16/60 Sephacryl S-200 HR column (GE)  
500 using 50 mM NaPi, 150 mM NaCl, pH 7.5 (Atu3277 SmoA; Atu3278, SmoB; Atu3279, SmoC) or  
501 50 mM sodium citrate, 150 mM NaCl, pH 5.5 (Atu3282, SmoF) as buffer (**Supplementary Fig. 2**).  
502 SmoI (Atu3285 or AtSQase) was prepared as previously described<sup>8</sup>.

503

#### 504 *SEC-MALS analyses*

505 Experiments were conducted on a system comprising a Wyatt HELEOS-II multi-angle light scattering  
506 detector and a Wyatt rEX refractive index detector linked to a Shimadzu LC system (SPD-20A UV  
507 detector, LC20-AD isocratic pump system, DGU-20A3 degasser and SIL-20A autosampler).  
508 Experiments were conducted at room temperature (20 ± 2°C). Solvents were filtered through a 0.2  
509 µm filter prior to use and a 0.1 µm filter was present in the flow path. The column was equilibrated  
510 with > 2 CV of buffer (50 mM NaPi, 300 mM NaCl pH 7.4) before use and buffer was infused at the  
511 working flow rate until baselines for UV, light scattering and refractive index detectors were all  
512 stable. The sample injection volume was 100 µl of protein at 6 mg ml<sup>-1</sup> in 50 mM NaPi buffer, 300  
513 mM NaCl pH 7.4. Shimadzu LC Solutions software was used to control the LC and Astra V software  
514 for the HELEOS-II and rEX detectors. The Astra data collection was 1 min shorter than the LC  
515 solutions run to maintain synchronization. Blank buffer injections were used as appropriate to check  
516 for carry-over between sample runs. Data were analyzed using the Astra V software. Molecular  
517 weights were estimated using the Zimm fit method with degree 1. A value of 0.158 was used for  
518 protein refractive index increment (dn/dc).

519

#### 520 *Isothermal Titration Calorimetry*

521 ITC experiments were performed using a MicroCal iTC200 (GE Healthcare) at 25 °C, with a 750  
522 r.p.m. stirring speed and a reference power of 10 µCal.s<sup>-1</sup>. Proteins and substrates were equilibrated  
523 into degassed and filter-sterilized buffer (50 mM NaPi, 200 mM NaCl, pH 7.4 for SmoC/F and 25  
524 mM NaPi, pH 7.5 for Smo B). Protein concentration was determined by BCA assay (Thermo Fisher)  
525 before initiating experiments. For SmoC–SQ binding, 600 µM SQ was titrated into the ITC cell

526 containing 40  $\mu\text{M}$  SmoC as a series of  $10 \times 3.94 \mu\text{l}$  injections with a pre-injection of  $1 \times 0.4 \mu\text{l}$ . For  
527 SmoF–SQGro binding, 200  $\mu\text{M}$  SQGro was titrated into the ITC cell containing 20  $\mu\text{M}$  SmoF as a  
528 series of  $15 \times 2.94 \mu\text{l}$  injections with a pre-injection of  $1 \times 0.4 \mu\text{l}$ . The delay between injections was  
529 set at 120 s, with an initial injection delay of 60 s. For SmoB–NAD(P)H binding, 1 mM NADH was  
530 titrated into the ITC cell containing 40  $\mu\text{M}$  SmoB as a series of  $19 \times 3 \mu\text{l}$  injections with a pre-injection  
531 of  $1 \times 4 \mu\text{l}$ . The delay between injections was set at 150 s, with an initial injection delay of 180 s. All  
532 data analysis was performed in MicroCal ITC Origin Analysis software (Malvern).

533

#### 534 *Nano Differential Scanning Fluorescence analysis of SmoF*

535 Thermal stability analysis for SmoF in the presence and absence of SQGro ligand was performed on  
536 a Prometheus NT.48 (NanoTemper) at 15% excitation, scanning from 20  $^{\circ}\text{C}$  to 65  $^{\circ}\text{C}$  at 0.5  $^{\circ}\text{C min}^{-1}$ .  
537 All protein samples were at a concentration of 1 mg  $\text{ml}^{-1}$  in 50 mM citrate, 150 mM NaCl at pH  
538 5.5, with a 10  $\mu\text{l}$  capillary load per sample. Data acquisition and analysis was performed with  
539 PR.ThermControl (NanoTemper) software.

540

#### 541 *Identification of the flavin co-factor that co-purified with SmoA*

542 100  $\mu\text{l}$  of recombinant flavin reductase (SmoA or RoSmoA) at a concentration of 20 mg  $\text{ml}^{-1}$  in 50  
543 mM Tris, 150 mM NaCl, pH 8.5 was heated at 90  $^{\circ}\text{C}$  for 10 min. The sample was clarified by  
544 centrifugation (16,000  $\times g$ , 10 min, 4  $^{\circ}\text{C}$ ) and the supernatant filtered (0.2  $\mu\text{m}$ ). Samples were analyzed  
545 by LCMS on an Agilent LCMS system (G6125B mass detector, 1290 Infinity G7120A high speed  
546 pump, 1290 Infinity G7129B autosampler, and 1290 Infinity G7117B diode array detector).  
547 Conditions for LC were as follows: column: Phenomenex 00B-4752-AN Luna Omega 1.6  $\mu\text{m}$  PS C<sub>18</sub>  
548 100 $\text{\AA}$  (50  $\times$  2.1 mm); injection volume: 1  $\mu\text{l}$ ; gradient: 3 to 100% B over 20 min (solvent A: water +  
549 0.1% FA; solvent B: MeCN + 0.1% FA); flow rate: 0.6 ml/min; DAD – 254 and 214 nm.

550

#### 551 *Michaelis-Menten kinetic analyses of SmoA and RoSmoA*

552 Reactions were conducted at 25  $^{\circ}\text{C}$  in 96-well plate format and involved the addition of SmoA or  
553 RoSmoA (final concentration of 20 nM for NADH and 500 nM for NADPH) to 20–800  $\mu\text{M}$   
554 NAD(P)H in 50 mM NaPi, 150 mM NaCl, 30  $\mu\text{M}$  FMN, 0.01% BSA, pH 7.4 at a total volume of  
555 100  $\mu\text{l}$ . The progress of the enzyme-catalyzed conversion of NAD(P)H to NAD(P)<sup>+</sup> was monitored  
556 by measuring loss of absorbance at 340 nm over time using an Envision Multimodal Plate Reader  
557 (Perkin Elmer). Initial rates for each reaction were calculated after first subtracting the rate of  
558 spontaneous NAD(P)H oxidation (determined using an enzyme-free control) and an empirically  
559 determined extinction coefficient for NAD(P)H under these conditions. Each initial rate was  
560 determined in triplicate and fit to a Michaelis-Menten equation using Prism 8 (GraphPad).

561

562 *Sulfoquinovose monooxygenase assay*

563 This SQ monooxygenase activity assay is based on a previously described alkanesulfonate  
564 monooxygenase activity assays<sup>18</sup> and uses Ellman's reagent to quantify sulfite released by these  
565 enzymes. A 2 ml reaction containing 1 mM SQ, 1 mM NADH, 3  $\mu$ M FMN, 0.01% (w/v) BSA, 100  
566 nM SmoA or *RoSmoA* and 300 nM SQ monooxygenase (SmoC or *RoSmoC*) in buffer (25 mM Tris  
567 pH 9.1, 25 mM NaCl) was incubated at 30 °C, along with controls lacking reaction components or  
568 using alternate sulfonate substrates. Reactions were initiated by the addition of SmoA or *RoSmoA* to  
569 the mixture. Sulfite concentration in the samples was determined at discrete time points by quenching  
570 40  $\mu$ l of the reaction in 160  $\mu$ l of Ellman's reagent (0.125 mg.ml<sup>-1</sup> in 25 mM NaPi pH 7.0, prepared  
571 fresh) within a 96-well plate. After 60 s, the absorbance of the sample at 405 nm was determined  
572 using an Envision Multimodal Plate Reader (Perkin Elmer). The sulfite concentration was  
573 interpolated using a calibration curve generated under these conditions: a linear relationship between  
574 sulfite concentration and absorbance at 405 nm was observed for 5–1000  $\mu$ M Na<sub>2</sub>SO<sub>3</sub>. The activity  
575 of SQ monooxygenases at different pH was determined by modifying the buffer in the above reactions  
576 (MES: pH 6.0, 6.5 and Tris: pH 7.0, 7.5, 8.0, 8.5, 9.1) using an endpoint of t = 30 min.

577

578 *Equilibrium isotope labelling using SmoB*

579 In order to pre-label the anomeric position, glucose was incubated in 98% H<sub>2</sub><sup>18</sup>O with heating at 80  
580 °C for 2 days, then evaporated to dryness to give C1-<sup>18</sup>O-labelled glucose. Labelling was determined  
581 to be 95% by mass spectrometry based on intensities of the M and M+2 peaks. Using H<sub>2</sub><sup>18</sup>O buffer  
582 (100 mM potassium phosphate, pH 7.0), NAD<sup>+</sup> and NADP<sup>+</sup> were each added at 0.05 molar equivalent  
583 to C1-<sup>18</sup>O-glucose and SmoB. Four control experiments were conducted: one without enzyme, one  
584 without NAD<sup>+</sup> and NADP<sup>+</sup>, one in H<sub>2</sub><sup>16</sup>O, and one in H<sub>2</sub><sup>16</sup>O with unlabeled glucose. Reactions were  
585 monitored by mass spectrometry. Only in the experimental sample containing enzyme, H<sub>2</sub><sup>18</sup>O and  
586 NAD<sup>+</sup>/NADP<sup>+</sup> was an M+4 signal observed and this reached a maximum intensity after 72 h. Two  
587 additional reactions were performed using SmoB, glucose and either NADP<sup>+</sup> or NAD<sup>+</sup> in H<sub>2</sub><sup>18</sup>O and  
588 only the reaction containing NADP<sup>+</sup> generated the M+4 species. To confirm that the M+4 species was  
589 glucose with two <sup>18</sup>O labels, we studied the product by HPLC. However, under aqueous HPLC  
590 conditions the <sup>18</sup>O-label at C1 is lost through chemical exchange with solvent. Therefore, we  
591 acetylated the product to form the pentaacetate to ensure no exchange at the anomeric position during  
592 HPLC analysis. The reaction mixture from above was evaporated under reduced pressure. The crude  
593 residue was treated with acetic anhydride in pyridine (1:2, 1 ml) overnight. The product was extracted  
594 with EtOAc and washed with sat. CuSO<sub>4</sub> to remove pyridine. The organic solution containing  
595 peracetylated glucose was analyzed by LCMS on an Agilent LCMS system (G6125B mass detector,

596 1290 Infinity G7120A high speed pump, 1290 Infinity G7129B autosampler, and 1290 Infinity  
597 G7117B diode array detector). Conditions for LC were as follows: column: Phenomenex 00B-4752-  
598 AN Luna Omega 1.6  $\mu\text{m}$  PS C<sub>18</sub> 100Å (50  $\times$  2.1 mm); injection volume: 1  $\mu\text{l}$ ; gradient: 0 to 65% B  
599 over 20 min (solvent A: water + 0.1% FA; solvent B: MeCN + 0.1% FA); flow rate: 0.6 ml/min. Peaks  
600 with  $m/z$  413 [M+Na]<sup>+</sup>,  $m/z$  415 [M+2+Na]<sup>+</sup>, and  $m/z$  417 [M+4+Na]<sup>+</sup> had the same retention time as  
601 an authentic glucose pentaacetate standard.

602

### 603 *GC-MS analysis of isotopically-labelled carbohydrates*

604 A 0.1  $\mu\text{l}$  aliquot of SmoB-glucose reaction mixture (containing  $\approx$ 2.5 nmol glucose) was transferred  
605 to a GC vial insert (deactivated) together with 1 nmol *scyllo*-inositol as an internal standard. Samples  
606 were derivatized as described in Antoniewicz *et al.*<sup>20</sup>, with minor modifications. Briefly, samples  
607 were dried (*in vacuo*, 35 °C with a 40  $\mu\text{l}$  methanol wash), followed by addition of hydroxylamine  
608 hydrochloride (20 mg ml<sup>-1</sup> in 25  $\mu\text{l}$  pyridine) and incubation at 90 °C for 1 h. Vials were cooled briefly  
609 at r.t. before the addition of propionic anhydride (50  $\mu\text{l}$ ) and incubation at 60 °C for 30 min. Samples  
610 were evaporated to dryness under a stream of nitrogen at 60 °C and resuspended in EtOAc (40  $\mu\text{l}$ ).  
611 Control samples of U-<sup>12</sup>C-glucose, U-<sup>13</sup>C-glucose, 1,2-<sup>13</sup>C<sub>2</sub>-glucose and 6,6-<sup>2</sup>H<sub>2</sub>-glucose were also  
612 prepared at a 2.5 nmol scale in the assay buffer mixture. Samples were blinded for analysis. The  
613 derivatized labelled glucose samples (**Supplementary Fig. 13** and **Supplementary Table 7**) were  
614 analyzed by GC-MS using a DB5 capillary column (J&W Scientific, 30 m, 250  $\mu\text{m}$  inner diameter,  
615 0.25  $\mu\text{m}$  film thickness) with a 10 m inert duraguard. The injector insert and GC-MS transfer line  
616 temperatures were 270 °C and 250 °C, respectively. The oven temperature gradient was programmed  
617 as follows: 70 °C (1 min); 70 °C to 295 °C at 12.5 °C min<sup>-1</sup>; 295 °C to 320 °C at 25 °C min<sup>-1</sup>; 320 °C  
618 for 2 min. Glucose and *scyllo*-inositol were identified by reference to authentic standards. A  
619 calibration curve was generated using glucose standard in assay buffer (starting concentration 50  
620 nmol, 2-fold dilution series). **Supplementary Fig. 12** shows the fraction of labelled fragments,  
621 corrected for isotope natural abundance by DExSI analysis<sup>39</sup>.

622

### 623 *Protein crystallization*

624 Initial crystallization screening was performed using commercially available INDEX (Hampton  
625 Research), PACT premier and CSSI/II (Molecular Dimensions) screens in 96-well sitting drop trays.  
626 Further optimization was carried out in a 48-well sitting drop or 24-well hanging-drop format to  
627 obtain optimal crystals for X-ray diffraction. Unless otherwise stated, all crystals were grown at 20  
628 °C.

629

630 Crystals of apo-SmoF were obtained by mixing 0.15  $\mu$ l of protein stock (50 mg ml<sup>-1</sup> protein in 50  
631 mM citrate, 150 mM NaCl, pH 5.5) with 0.15  $\mu$ l mother liquor (0.3 M ammonium acetate, 0.1 M Bis-  
632 Tris, 25% w/v PEG 3350, pH 5.5) housed in a Rigaku Xtaltrak plate hotel to enable consistent growth  
633 and monitoring at 6 °C. Crystals were harvested with nylon CryoLoops<sup>TM</sup> (Hampton Research) and  
634 cryopreserved in liquid nitrogen without additional cryoprotectants.

635

636 Crystals of SmoF were initially obtained by mixing 0.15  $\mu$ l of protein stock (3.5 mg ml<sup>-1</sup> protein with  
637 2'R-SQGro at a 1:10 molar ratio in 50 mM citrate, 150 mM NaCl, pH 5.5) with 0.15  $\mu$ l mother liquor  
638 (30% (w/v) polyethylene glycol 4000, 0.2 M sodium acetate, 0.1 M tris chloride, pH 8.5). The  
639 resulting crystals were used to prepare a seed stock by mixing the crystallization drop with 100  $\mu$ l  
640 mother liquor and vortexing for 60 s with one teflon bead. An optimisation plate was setup with drops  
641 comprised of 0.1  $\mu$ l of various mother liquors (28-36% (w/v) polyethylene glycol 4000, 0.2 M sodium  
642 acetate, 0.1 M tris chloride, pH 7.1-9.1), 50 nl seed stock solution, and 0.15  $\mu$ l protein stock (4 mg  
643 ml<sup>-1</sup> protein with 2'R-SQGro at a 1:10 molar ratio in 50 mM citrate, 150 mM NaCl, pH 5.5). A single  
644 crystal grown at 31.8% (w/v) polyethylene glycol 4000, 0.2 M sodium acetate, 0.1 M tris chloride,  
645 pH 8.95, was harvested with a nylon CryoLoop<sup>TM</sup> (Hampton Research) and cryopreserved in liquid  
646 nitrogen with 25% (v/v) ethylene glycol as cryoprotectant.

647

648 Crystals of SmoI-D455N-E370A-E371A were obtained by mixing 0.4  $\mu$ l of protein stock (35 mg ml<sup>-1</sup>  
649 <sup>1</sup> protein in 50 mM NaPi, 300 mM NaCl, pH 7.4) with 0.5  $\mu$ l mother liquor (26% PEG 3350 w/v, 0.2  
650 M KSCN, 0.1 M Bis-Tris propane, pH 6.5). Crystals were soaked with solid SQGro in mother liquor  
651 for 2 min prior to harvesting with nylon CryoLoops<sup>TM</sup> (Hampton Research) and cryopreserved  
652 without additional cryoprotectants.

653

654 Crystals of apo-SmoC were obtained by mixing 0.6  $\mu$ l of protein stock (60 mg ml<sup>-1</sup> protein in 50 mM  
655 Tris, 300 mM NaCl, pH 7.5) with 0.5  $\mu$ l mother liquor (0.2 M NaCl, 0.1 M MES pH 6, 26% PEG  
656 6000 w/v and 10 mM SQ-glucitol). Crystals of apo-RoSmoC were obtained by mixing 0.1  $\mu$ l of  
657 protein stock (11.7 mg ml<sup>-1</sup> protein in 50 mM Tris, 300 mM NaCl, pH 7.5) with 0.2  $\mu$ l mother liquor  
658 (0.2M NaNO<sub>3</sub>, 20% PEG 3350 w/v and 10 mM SQ). Crystals were harvested with nylon  
659 CryoLoops<sup>TM</sup> (Hampton Research) and cryopreserved in liquid nitrogen without additional  
660 cryoprotectants.

661

662 Crystals of SmoB-apo (YSBLIC3C construct) were obtained by mixing 0.15  $\mu$ l of protein stock (20  
663 mg ml<sup>-1</sup> protein in 50 mM NaPi, 150 mM NaCl, pH 7.4) with 0.15  $\mu$ l mother liquor (0.2 M sodium  
664 malonate dibasic monohydrate, 0.1 M Bis-Tris propane pH 8.5, 20% w/v PEG 3350). For the

665 SmoB•NADPH complex, crystals were obtained by mixing 0.15  $\mu$ l of protein stock (20 mg ml<sup>-1</sup>  
666 protein in 50 mM NaPi, 150 mM NaCl, 2 mM NADPH, pH 7.4) with 0.15  $\mu$ l mother liquor (0.1 M  
667 succinic acid, sodium dihydrogen phosphate, glycine buffer (SPG buffer, Qiagen), 25% w/v PEG  
668 1500 at pH 6.0). For the SmoB•NADPH•Glc complex, crystals were obtained in a hanging drop by  
669 mixing 1  $\mu$ l of protein stock (13 mg ml<sup>-1</sup> protein in 50 mM NaPi 150 mM NaCl, pH 7.4) with 1  $\mu$ l of  
670 mother liquor (2 mM NADPH, 0.1 M SPG (Qiagen), 25% w/v PEG 1500 at pH 6). Crystals were  
671 soaked with solid glucose in mother liquor for 1 min prior to harvesting with nylon CryoLoops™  
672 (Hampton Research) and cryopreserved without additional cryoprotectants.

673

#### 674 *X-ray data collection, processing and refinement*

675 The data were processed and integrated using XDS<sup>40</sup> and scaled using SCALA<sup>41</sup> included in the Xia2  
676 processing system<sup>42</sup>. Data reduction was performed with AIMLESS, and resolution was cut until  
677 CC1/2 = 0.5. The structure of the SmoI•SQGro complex was determined using molecular replacement  
678 using 5OHS<sup>8</sup> as the initial model. For SmoF, the structure was solved by molecular replacement using  
679 PHASER<sup>43</sup> with a search model created from PDB ID: 6DTQ<sup>44</sup>. The structure of RoSmoC was solved  
680 by molecular replacement using the ensemble based on PDB ID: 1M41<sup>18</sup> as an initial search model.  
681 The structure of SmoB was determined using molecular replacement with the monomer of an aldo-  
682 keto reductase from *S. enterica* (PDB ID: 4R9O) as the initial model. The apo-SmoF structure was  
683 solved using a dissected C-terminal domain of the SmoF•SQGro structure. Structures were built and  
684 refined by iterative cycles using Coot<sup>45</sup> and REFMAC<sup>46</sup> or Phenix,<sup>47</sup> the latter employing local NCS  
685 restraints. Following building and refinement of the protein and water molecules, clear residual  
686 density was observed in the omit maps for co-complex structures, respective ligands were modelled  
687 into these. The coordinate and refinement library files were prepared using ACEDRG<sup>48</sup>. The final  
688 structures gave  $R_{\text{cryst}}$  and  $R_{\text{free}}$  values along with data and refinement statistics that are presented in  
689 **Supplementary Table 4-6**. Data were collected at Diamond light source, Didcot, Oxfordshire, U.K.,  
690 on beamlines I24 (SmoI-D455N•SQGro, to 2.15 Å; SmoF-apo, to 1.88 Å), I04 (RoSmoC to 1.75 Å)  
691 and I04-1 (SmoC-apo, to 3.2 Å; SmoB-apo\_YSBLIC3C, to 1.5 Å; SmoB-apo; pET29a;  
692 SmoB•NADPH and SmoB•NADPH•Glc) and at the Australian Synchrotron using the MX2 beamline  
693 (At3282•SQGro complex, to 1.7 Å). The coordinate files and structure factors have been deposited  
694 in the Protein DataBank (PDB) with the coordinate accession numbers 7OFX (SmoI-D455N•SQGro),  
695 7NBZ (SmoF-apo), 7OFY (SmoF•SQGro), 7OH2 (RoSmoC), 7OLF (SmoC-apo), 7BBY (SmoB-  
696 apo; pET29a), 7BBZ (SmoB-apo; YSBLIC3C), 7BC0 (SmoB•NADPH) and 7BC1  
697 (SmoB•NADPH•Glc).

698

#### 699 *Structure-based analyses*

700 Crystal packing interactions were analyzed using the protein interactions, surfaces, and assemblies  
701 (PISA) server.<sup>49</sup> Structural comparisons and structure-based sequence alignments were conducted  
702 using PDB25 search on DALI server against a representative subset of the Protein Data Bank<sup>50</sup>. All  
703 structure figures were generated using ccp4mg<sup>51</sup>.

704

#### 705 *Bioinformatic analysis SMO pathway prevalence*

706 Each gene within the *A. tumefaciens* C58 SMO gene cluster (*Atu3277-Atu3285*) was submitted as a  
707 query to the NCBI BLASTp algorithm to search a database comprised of non-redundant protein  
708 sequences with *A. tumefaciens* (taxid: 358) sequences excluded. Standard algorithm parameters were  
709 used, except the maximum target sequences was set to 10,000. Results were filtered to only retain  
710 protein sequences with E-value  $\leq 1.19 \times 10^{-51}$ . The corresponding nucleotide accession numbers for  
711 each protein from all nine searches were extracted, combined and duplicates removed to provide a  
712 list of candidate genome sequences. This was converted into a reference library for  
713 MultiGeneBLAST<sup>52</sup> and queried using the *A. tumefaciens* C58 SMO gene cluster. Clusters identified  
714 by this workflow with both an SQ monooxygenase and SQase homolog were regarded as putative  
715 SMO gene clusters. Clusters representative of the observed diversity were visualized using Clinker<sup>53</sup>.  
716 A phylogenetic tree of species possessing a putative SMO gene cluster was generated by pruning the  
717 All-Species Living Tree Project's 16s rRNA release 132<sup>54</sup> using iTOL<sup>55</sup>.

718

#### 719 **Data Availability Statement**

720 All relevant data are available from the authors upon request. Structure coordinates have been  
721 deposited in the Protein Data Bank (<https://www.rcsb.org/>) under accession codes 7OFX, 7OFY,  
722 7NBZ, 7OH2, 7OLF, 7BBZ, 7BC0, 7BC1 and 7BBY. Proteomics data are available via  
723 ProteomeXchange<sup>56</sup> (<http://www.proteomexchange.org/>) with the identifier PXD014115.

724

725 **References**

- 726 1. Goddard-Borger, E.D. & Williams, S.J. Sulfoquinovose in the biosphere: occurrence,  
727 metabolism and functions. *Biochem. J.* **474**, 827–849 (2017).
- 728 2. Harwood, J.L. & Nicholls, R.G. The plant sulpholipid - a major component of the sulphur  
729 cycle. *Biochem. Soc. Trans.* **7**, 440-447 (1979).
- 730 3. Denger, K. et al. Sulphoglycolysis in *Escherichia coli* K-12 closes a gap in the  
731 biogeochemical sulphur cycle. *Nature* **507**, 114-117 (2014).
- 732 4. Felux, A.K., Spittler, D., Klebensberger, J. & Schleheck, D. Entner-Doudoroff pathway for  
733 sulfoquinovose degradation in *Pseudomonas putida* SQ1. *Proc. Natl. Acad. Sci. USA* **112**,  
734 E4298-305 (2015).
- 735 5. Li, J. et al. A Sulfoglycolytic Entner-Doudoroff Pathway in *Rhizobium leguminosarum* bv.  
736 *trifolii* SRDI565. *Appl. Environ. Microbiol.* **86**, e00750-20 (2020).
- 737 6. Frommeyer, B. et al. Environmental and Intestinal Phylum Firmicutes Bacteria Metabolize  
738 the Plant Sugar Sulfoquinovose via a 6-Deoxy-6-sulfofructose Transaldolase Pathway.  
739 *iScience* **23**, 101510 (2020).
- 740 7. Liu, Y. et al. A transaldolase-dependent sulfoglycolysis pathway in *Bacillus megaterium*  
741 DSM 1804. *Biochem. Biophys. Res. Commun.* **533**, 1109-1114 (2020).
- 742 8. Abayakoon, P. et al. Structural and Biochemical Insights into the Function and Evolution of  
743 Sulfoquinovosidases. *ACS Cent. Sci.* **4**, 1266-1273 (2018).
- 744 9. Speciale, G., Jin, Y., Davies, G.J., Williams, S.J. & Goddard-Borger, E.D. YihQ is a  
745 sulfoquinovosidase that cleaves sulfoquinovosyl diacylglyceride sulfolipids. *Nat. Chem.*  
746 *Biol.* **12**, 215-217 (2016).
- 747 10. Roy, A.B., Hewlins, M.J., Ellis, A.J., Harwood, J.L. & White, G.F. Glycolytic breakdown of  
748 sulfoquinovose in bacteria: a missing link in the sulfur cycle. *Appl. Environ. Microbiol.* **69**,  
749 6434-6441 (2003).
- 750 11. Kertesz, M.A. Riding the sulfur cycle - metabolism of sulfonates and sulfate esters in Gram-  
751 negative bacteria. *FEMS Microbiol. Rev.* **24**, 135-175 (2000).
- 752 12. Abayakoon, P. et al. Comprehensive synthesis of substrates, intermediates and products of  
753 the sulfoglycolytic Embden-Meyerhoff-Parnas pathway. *J. Org. Chem.* **84**, 2910-2910  
754 (2019).
- 755 13. Speers, A.E. & Wu, C.C. Proteomics of Integral Membrane Proteins: Theory and  
756 Application. *Chem. Rev.* **107**, 3687-3714 (2007).
- 757 14. Davidson, A.L., Dassa, E., Orelle, C. & Chen, J. Structure, Function, and Evolution of  
758 Bacterial ATP-Binding Cassette Systems. *Microbiol. Mol. Biol. Rev.* **72**, 317-364 (2008).

- 759 15. van Der Ploeg, J.R., Iwanicka-Nowicka, R., Bykowski, T., Hryniewicz, M.M. & Leisinger,  
760 T. The *Escherichia coli* ssuEADCB gene cluster is required for the utilization of sulfur from  
761 aliphatic sulfonates and is regulated by the transcriptional activator Cbl. *J. Biol. Chem.* **274**,  
762 29358-65 (1999).
- 763 16. Thakur, A. et al. Substrate-Dependent Mobile Loop Conformational Changes in  
764 Alkanesulfonate Monooxygenase from Accelerated Molecular Dynamics. *Biochemistry* **59**,  
765 3582-3593 (2020).
- 766 17. Liew, J.J.M., El Saudi, I.M., Nguyen, S.V., Wicht, D.K. & Dowling, D.P. Structures of the  
767 alkanesulfonate monooxygenase MsuD provide insight into C-S bond cleavage, substrate  
768 scope, and an unexpected role for the tetramer. *J. Biol. Chem.* **297**(2021).
- 769 18. Eichhorn, E., Davey, C.A., Sargent, D.F., Leisinger, T. & Richmond, T.J. Crystal Structure  
770 of *Escherichia coli* Alkanesulfonate Monooxygenase SsuD. *J. Mol. Biol.* **324**, 457-468  
771 (2002).
- 772 19. Li, L. et al. Crystal structure of long-chain alkane monooxygenase (LadA) in complex with  
773 coenzyme FMN: unveiling the long-chain alkane hydroxylase. *J. Mol. Biol.* **376**, 453-65  
774 (2008).
- 775 20. Antoniewicz, M.R., Kelleher, J.K. & Stephanopoulos, G. Measuring deuterium enrichment  
776 of glucose hydrogen atoms by gas chromatography/mass spectrometry. *Anal. Chem.* **83**,  
777 3211-6 (2011).
- 778 21. Penning, T.M. The aldo-keto reductases (AKRs): Overview. *Chem. Biol. Interact.* **234**, 236-  
779 46 (2015).
- 780 22. Dippel, R. & Boos, W. The Maltodextrin System of *Escherichia coli*: Metabolism and  
781 Transport. *J. Bacteriol.* **187**, 8322 (2005).
- 782 23. Sharma, M. et al. Dynamic Structural Changes Accompany the Production of  
783 Dihydroxypropanesulfonate by Sulfolactaldehyde Reductase. *ACS Catalysis* **10**, 2826-2836  
784 (2020).
- 785 24. Sharma, M. et al. Molecular Basis of Sulfosugar Selectivity in Sulfoglycolysis. *ACS Cent.*  
786 *Sci.* **7**, 476-487 (2021).
- 787 25. Udvardi, M. & Poole, P.S. Transport and metabolism in legume-rhizobia symbioses. *Annu.*  
788 *Rev. Plant Biol.* **64**, 781-805 (2013).
- 789 26. Speck, J.J., James, E.K., Sugawara, M., Sadowsky, M.J. & Gyaneshwar, P. An Alkane  
790 Sulfonate Monooxygenase Is Required for Symbiotic Nitrogen Fixation by *Bradyrhizobium*  
791 *diazoefficiens* (syn. *Bradyrhizobium japonicum*) USDA110(T). *Appl. Environ. Microbiol.*  
792 **85**(2019).

- 793 27. Denger, K., Huhn, T., Hollemeyer, K., Schleheck, D. & Cook, A.M. Sulfoquinovose  
794 degraded by pure cultures of bacteria with release of C<sub>3</sub>-organosulfonates: complete  
795 degradation in two-member communities. *FEMS Microbiol. Lett.* **328**, 39-45 (2012).
- 796 28. Blakeney, A.B. & Mutton, L.L. A simple colorimetric method for the determination of  
797 sugars in fruit and vegetables. *J. Sci. Food Agric.* **31**, 889-897 (1980).
- 798 29. Sörbo, B. Sulfate: Turbidimetric and nephelometric methods. in *Methods Enzymol.*, Vol.  
799 143 3-6 (Academic Press, 1987).
- 800 30. Brychkova, G., Yarmolinsky, D., Fluhr, R. & Sagi, M. The determination of sulfite levels  
801 and its oxidation in plant leaves. *Plant Sci.* **190**, 123-130 (2012).
- 802 31. Kurmanbayeva, A. et al. Determination of Total Sulfur, Sulfate, Sulfite, Thiosulfate, and  
803 Sulfolipids in Plants. in *Plant Stress Tolerance: Methods and Protocols* (ed. Sunkar, R.)  
804 253-271 (Springer New York, New York, NY, 2017).
- 805 32. Scott, N.E. et al. Simultaneous glycan-peptide characterization using hydrophilic interaction  
806 chromatography and parallel fragmentation by CID, higher energy collisional dissociation,  
807 and electron transfer dissociation MS applied to the N-linked glycoproteome of  
808 *Campylobacter jejuni*. *Mol. Cell. Proteomics* **10**, M000031-mcp201 (2011).
- 809 33. Rappsilber, J., Mann, M. & Ishihama, Y. Protocol for micro-purification, enrichment, pre-  
810 fractionation and storage of peptides for proteomics using StageTips. *Nat. Protoc.* **2**, 1896-  
811 1906 (2007).
- 812 34. Cox, J. & Mann, M. MaxQuant enables high peptide identification rates, individualized  
813 p.p.b.-range mass accuracies and proteome-wide protein quantification. *Nat. Biotechnol.* **26**,  
814 1367-1372 (2008).
- 815 35. Cox, J. et al. Accurate Proteome-wide Label-free Quantification by Delayed Normalization  
816 and Maximal Peptide Ratio Extraction, Termed MaxLFQ. *Mol. Cell. Proteomics* **13**, 2513  
817 (2014).
- 818 36. Tyanova, S. et al. Visualization of LC-MS/MS proteomics data in MaxQuant. *Proteomics*  
819 **15**, 1453-6 (2015).
- 820 37. Perez-Riverol, Y. et al. The PRIDE database and related tools and resources in 2019:  
821 improving support for quantification data. *Nucleic Acids Res.* **47**, D442-d450 (2019).
- 822 38. Fogg, Mark J. & Wilkinson, Anthony J. Higher-throughput approaches to crystallization and  
823 crystal structure determination. *Biochem. Soc. Trans.* **36**, 771-775 (2008).
- 824 39. Dagley, M.J. & McConville, M.J. DExSI: a new tool for the rapid quantitation of <sup>13</sup>C-  
825 labelled metabolites detected by GC-MS. *Bioinformatics* **34**, 1957-1958 (2018).
- 826 40. Kabsch, W. Xds. *Acta Crystallogr., Section D: Biol. Crystallogr.* **66**, 125-132 (2010).

- 827 41. Evans, P. Scaling and assessment of data quality. *Acta Crystallogr. Sect. D* **62**, 72-82  
828 (2006).
- 829 42. Winter, G. xia2: an expert system for macromolecular crystallography data reduction. *J.*  
830 *Appl. Crystallogr.* **43**, 186-190 (2010).
- 831 43. Storoni, L.C., McCoy, A.J. & Read, R.J. Likelihood-enhanced fast rotation functions. *Acta*  
832 *Crystallogr. D Biol. Crystallogr.* **60**, 432-8 (2004).
- 833 44. Shukla, S. et al. Differential Substrate Recognition by Maltose Binding Proteins Influenced  
834 by Structure and Dynamics. *Biochemistry* **57**, 5864-5876 (2018).
- 835 45. Emsley, P. & Cowtan, K. Coot: Model-building tools for molecular graphics. *Acta*  
836 *Crystallogr., Sect. D: Biol. Crystallogr.* **60**, 2126-2132 (2004).
- 837 46. Murshudov, G.N., Vagin, A.A. & Dodson, E.J. Refinement of Macromolecular Structures  
838 by the Maximum-Likelihood Method. *Acta Crystallogr. Sect. D* **53**, 240-255 (1997).
- 839 47. Adams, P.D. et al. PHENIX: a comprehensive Python-based system for macromolecular  
840 structure solution. *Acta Crystallogr. D Biol. Crystallogr.* **66**, 213-21 (2010).
- 841 48. Long, F. et al. AceDRG: a stereochemical description generator for ligands. *Acta*  
842 *Crystallogr. Sect. D* **73**, 112-122 (2017).
- 843 49. Krissinel, E. & Henrick, K. Secondary-structure matching (SSM), a new tool for fast protein  
844 structure alignment in three dimensions. *Acta Crystallogr. D* **60**, 2256-2268 (2004).
- 845 50. Holm, L. & Rosenström, P. Dali server: conservation mapping in 3D. *Nucleic Acids Res.* **38**,  
846 W545-W549 (2010).
- 847 51. McNicholas, S., Potterton, E., Wilson, K.S. & Noble, M.E.M. Presenting your structures:  
848 the CCP4mg molecular-graphics software. *Acta Crystallogr. D* **67**, 386-394 (2011).
- 849 52. Medema, M.H., Takano, E. & Breitling, R. Detecting sequence homology at the gene cluster  
850 level with MultiGeneBlast. *Mol. Biol. Evol.* **30**, 1218-23 (2013).
- 851 53. Gilchrist, C.L.M. & Chooi, Y.H. Clinker & clustermap.js: Automatic generation of gene  
852 cluster comparison figures. *Bioinformatics* (2021).
- 853 54. Yilmaz, P. et al. The SILVA and “All-species Living Tree Project (LTP)” taxonomic  
854 frameworks. *Nucl. Acids Res.* **42**, D643-D648 (2013).
- 855 55. Letunic, I. & Bork, P. Interactive Tree Of Life (iTOL) v4: recent updates and new  
856 developments. *Nucl. Acids Res.* **47**, W256-W259 (2019).
- 857 56. Deutsch, E.W. et al. The ProteomeXchange consortium in 2017: supporting the cultural  
858 change in proteomics public data deposition. *Nucl. Acids Res.* **45**, D1100-D1106 (2016).

859  
860

861 **Acknowledgements**

862 Dr Monica Doblin is thanked for the provision of *Agrobacterium tumefaciens* strain C58. This work  
863 was supported in part by National Health and Medical Research Council of Australia (NHMRC)  
864 project grants GNT1100164 (N.E.S), GNT1174405 (D.B.A.), GNT1139546 and GNT1139549  
865 (E.D.G.-B); the Leverhulme Trust grant RPG-2017-190 (G.J.D.); Australian Research Council grant  
866 DP180101957 and DP210100233 (S.J.W.), and DP210100362 (N.E.S.); and support from The Walter  
867 and Eliza Hall Institute of Medical Research, the Australian Cancer Research Fund and a Victorian  
868 State Government Operational Infrastructure support grant (E.D.G.-B). G.J.D is supported by the  
869 Royal Society Ken Murray Research Professorship, E.D.G.-B. is supported by the Brian M. Davis  
870 Charitable Foundation Centenary Fellowship, M.J.M. is an NHMRC Principal Research Fellow,  
871 N.E.S. is supported by and Australian Research Council Future Fellowship (FT200100270), B.M.  
872 was supported by Melbourne Research Scholarship, J.M. by a Sir John and Lady Higgins Scholarship,  
873 M.P. by an Australian Postgraduate Award. We acknowledge Dr. Johan P. Turkenburg and Sam Hart  
874 for assistance with X-ray data collection; the Diamond Light Source for access to beamlines I04, i24  
875 and I04-1 under proposal number mx-18598; and the Australian Synchrotron, part of ANSTO, for  
876 access to the MX-2 beamline, which made use of the Australian Cancer Research Foundation (ACRF)  
877 detector. We thank the ‘Melbourne Mass Spectrometry and Proteomics Facility’ of the Bio21  
878 Molecular Science and Biotechnology Institute at The University of Melbourne for the support of  
879 mass spectrometry analysis and the ‘Bioscience Technology Facility’ (University of York) for  
880 assistance with SEC-MALS analyses.

881

882 **Author Contributions**

883 EDG-B discovered the SMO gene cluster; SJW, EDG-B, GJD conceived project; MP and JW-YM  
884 conducted microbial growth experiments; NES conducted proteomics; JPL, MS, AS, MJ performed  
885 molecular biology, protein expression and structural and biophysical characterization; YZ, JPL, AS,  
886 MS, RM performed biochemical assays; ECS and MJM conducted carbohydrate analysis; YZ, JW-  
887 YM, BM and DA performed bioinformatics analysis; SJW, MS, EGB wrote the paper with input from  
888 all authors.

889

890 **Competing Financial Interests Statement**

891 The authors declare no competing interests.

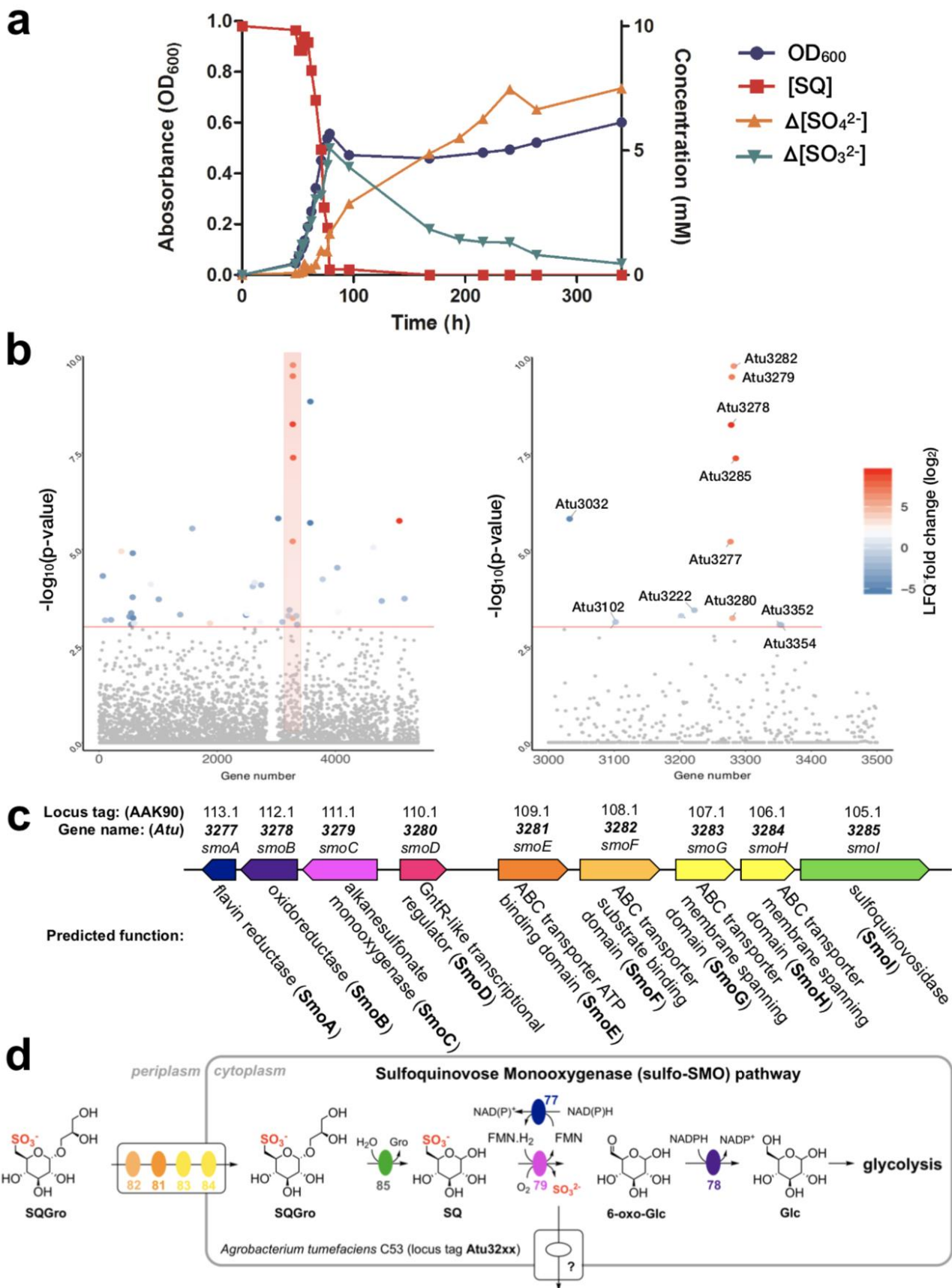
892

893 **Additional information**

894 Supplementary information

895 Correspondence and requests for materials should be addressed to S.J.W, G.J.D or E.D.G.-B.

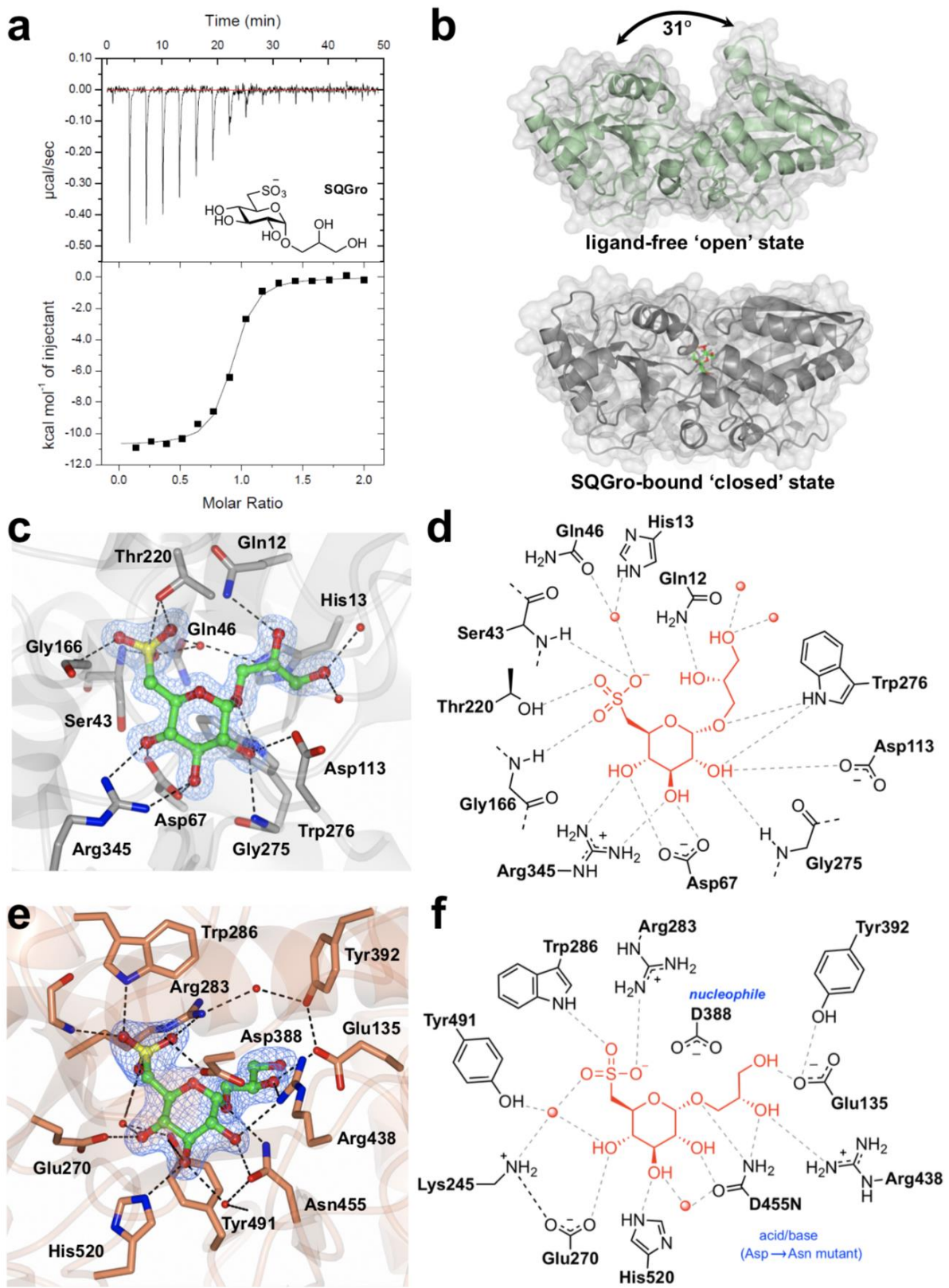
896



897

898 **Figure 1: *A. tumefaciens* utilizes SQ and its glycosides as a carbon source.** (a) Optical density of  
 899 *A. tumefaciens* C58 culture (blue) and [SQ] (red), change in [sulfite] (green) and change in [sulfate]  
 900 (yellow), with respect to time. (b) Manhattan plot of comparative proteomics data for *A. tumefaciens*

901 C58 grown on SQ vs glucose, demonstrating that the most heavily upregulated proteins belong to a  
902 single gene cluster. (c) A cartoon of the upregulated cluster with automated annotations for each of  
903 the gene products. These would later be renamed *smoABCDEFGHI*, to reflect the importance of the  
904 sulfoquinovose monooxygenase enzyme activity to this new biochemical pathway. (d) A cartoon  
905 illustrating the hypothetical roles played by the gene products of this pathway to complete the  
906 catabolism of SQGro.



907

908

909

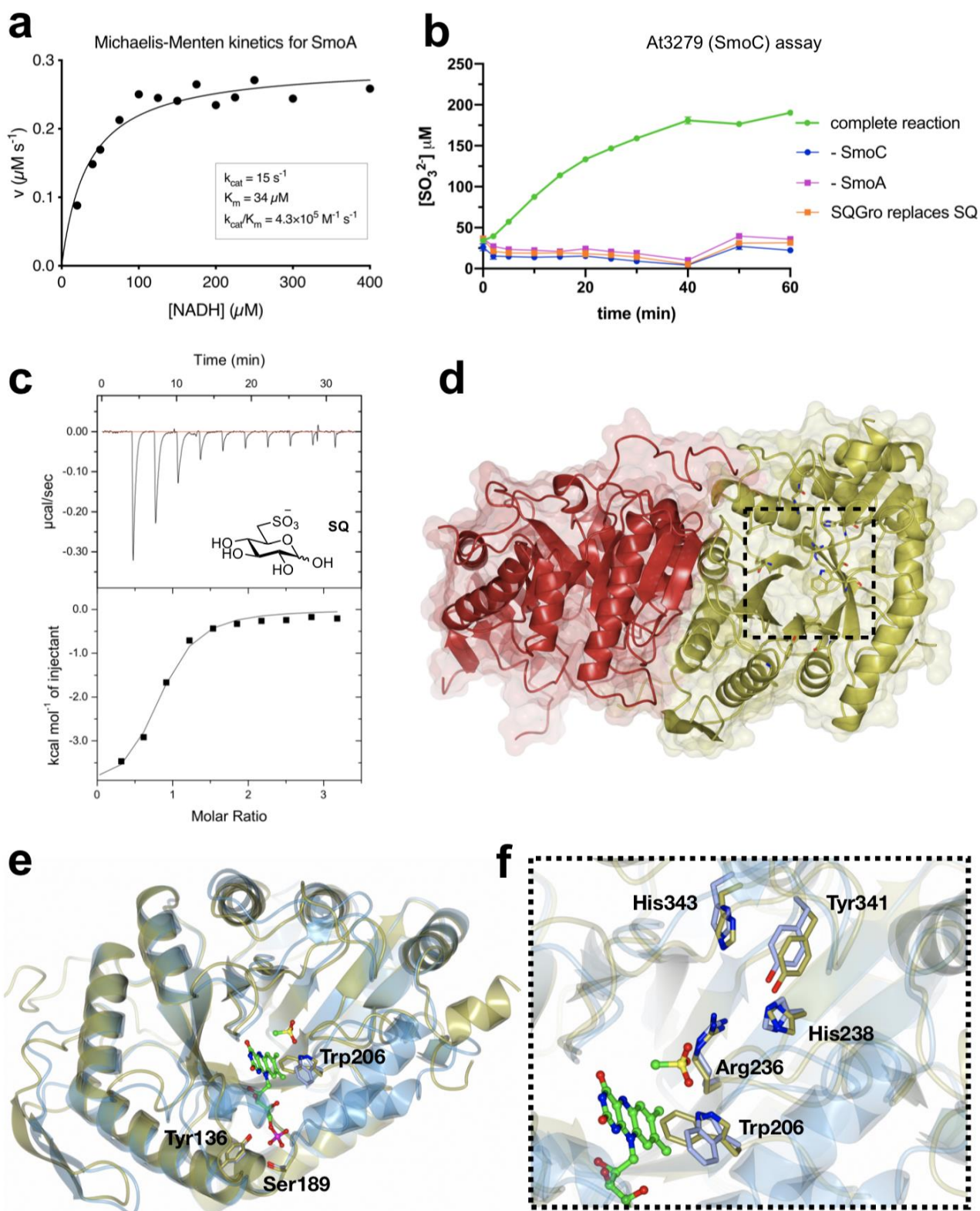
910

911

912

**Figure 2: Biochemical and structural analyses of the SQGro-binding protein SmoF (Atu3282) and SQase SmoI (Atu3285).** (a) A representative ITC isotherm for SmoF titrated against its cognate ligand 2'R-SQGro. (b) Ribbon diagrams (with transparent surface) for the open and closed (liganded) conformations of SmoF. 2'R-SQGro is bound tightly in the inter-domain cleft and is inaccessible to the bulk solvent in the closed conformation. (c) Interactions between protein and ligand within the

913 SmoF•2'R-SQGro complex: SmoF is in grey, 2'R-SQGro is in green, and the 2Fo – Fc map at 1.5σ  
914 is in blue. (d) A cartoon highlighting key interactions from c. (e) Interactions between protein and  
915 ligand within the complex pf SmoI-D455N SQase and 2'R-SQGro: SmoI is in gold, 2'R-SQGro is in  
916 green, and the 2Fo – Fc map at 1.5σ is in blue. (f) A cartoon highlighting key interactions from e: red  
917 spheres represent ordered water molecules; dotted lines represent proposed hydrogen bonds.  
918



919

920

921

922

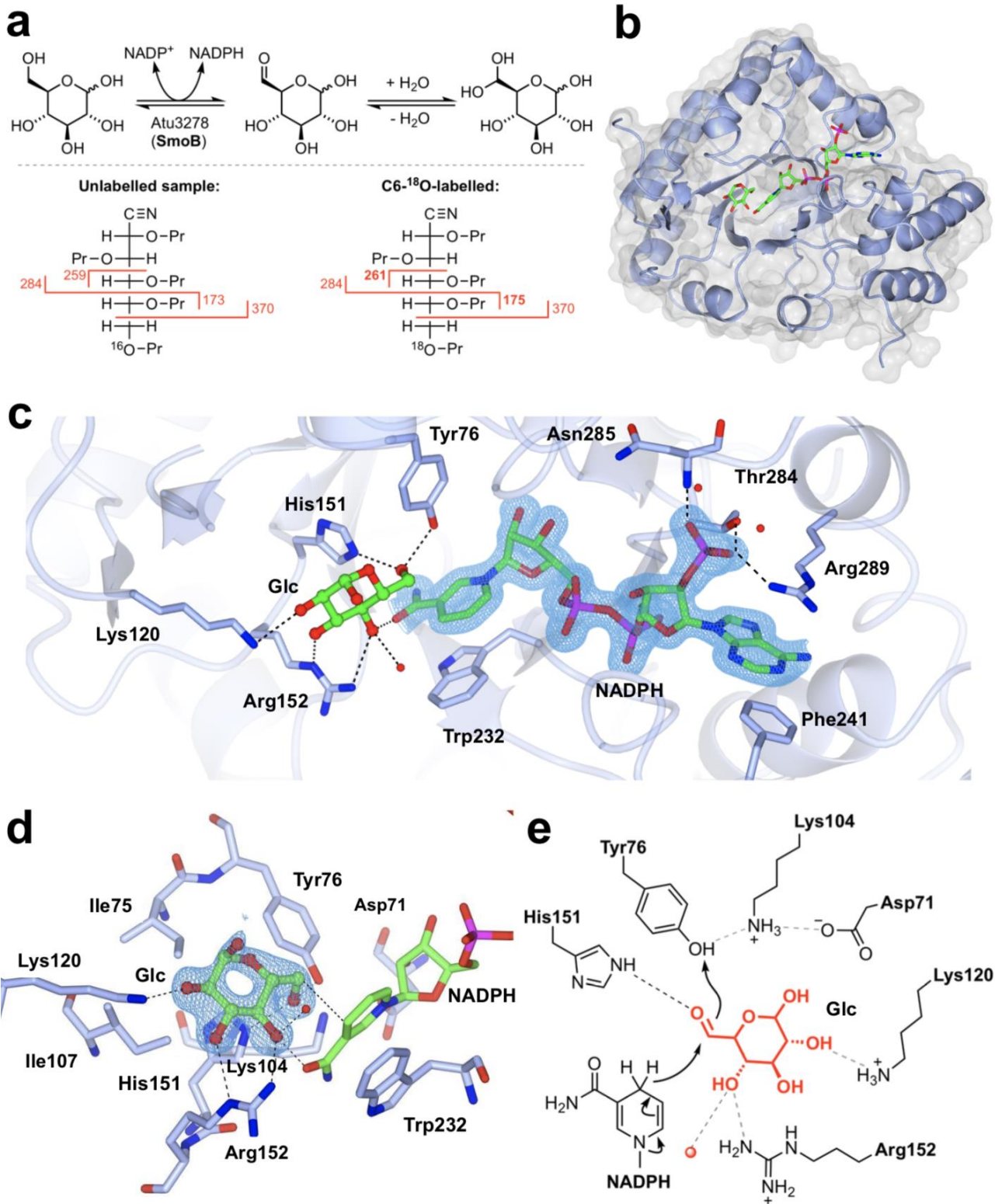
923

924

925

**Figure 3: Biochemical and structural analyses of the flavin reductase SmoA and SQ monooxygenase SmoC.** (a) Michaelis-Menten kinetics for SmoA-catalysed reduction of FMN by NADH (b) SmoC activity assessed using sulfite release assay with Ellman's reagent in the presence of FMN, flavin reductase, NADH and SQ. (c) Isothermal titration calorimogram of interaction of SmoC with SQ as determined by ITC. (d) Transparent molecular surface and ribbon diagram of *RoSmoC* homodimer showing cofactor binding pocket and active site. (e) Overlay of *RoSmoC* (in

926 gold) and LadA·FMN complex (3B9O.pdb in ice blue) showing location of FMN pocket. (f) Overlay  
927 of *RoSmoC* (in gold) and SsuD (1M41.pdb in grey) showing detailed view of proposed substrate-  
928 binding pocket and conserved residues lining the active site of *RoSmoC*.



929

930

931

932

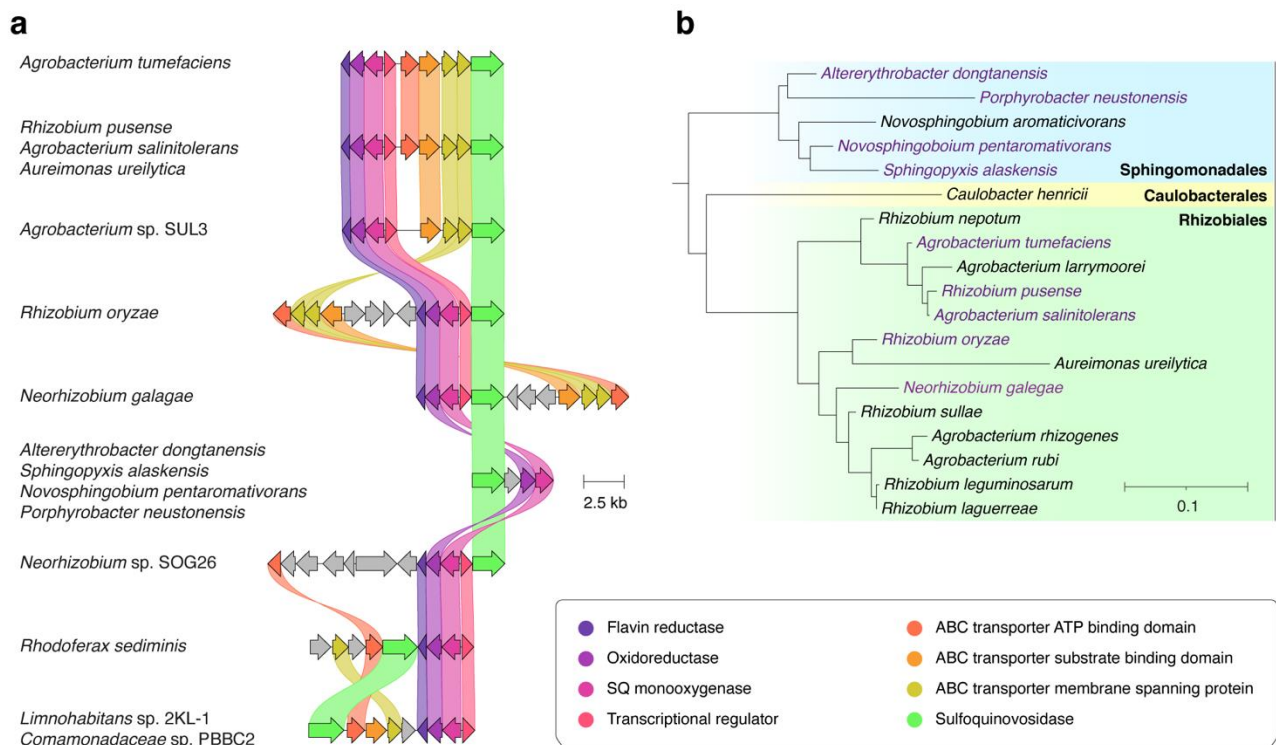
933

934

935

**Figure 4: Biochemical and structural analyses of 6-oxo-glucose reductase SmoB.** (a) Top: Equilibrium oxygen exchange at C-6 of Glc via 6-OG facilitated by SmoB when incubated with NADP<sup>+</sup> in H<sub>2</sub><sup>18</sup>O. Bottom: Derivatization and MS fragmentation allows localization of <sup>18</sup>O to C6 of Glc. (b) Transparent molecular surface and ribbon diagram of SmoB in complex with NADPH and Glc. (c) Closeup view of SmoB•NADPH•Glc ternary complex. Backbone and carbon atoms of SmoB are shown in ice blue and NADPH and glucose are shown in cylinder format. Electron density for

936 NADPH corresponds to the 2Fo – Fc map in blue at levels of 1 $\sigma$ . (d) Substrate binding pocket of  
937 SmoB depicting hydrogen bonding interactions of glucose with the active site residues including the  
938 conserved catalytic residues Asp71, Lys 104, His151 and Tyr76. Electron density corresponds to the  
939 2Fo – Fc map (in blue) at levels of 1 $\sigma$ . The geometry of the SmoB-Glc complex indicates the likely  
940 trajectory of hydride addition to 6-OG. (e) Proposed mechanism of SmoB catalyzed reduction of 6-  
941 OG by NADPH showing hydride transfer from C4 of nicotinamide ring of NADPH to C6 carbonyl  
942 and Y76 (within the catalytic tetrad) as the proton donor. The red sphere is a bound water molecule;  
943 dotted lines are proposed hydrogen bonds.



944

945 **Figure 5: Prevalence of the SMO pathway.** (a) Architecture of the SMO gene cluster in *A.*  
 946 *tumefaciens* and homologous gene clusters in other organisms. Colored links indicate  $\geq 30\%$  protein  
 947 sequence similarity. Only those clusters encoding putative SQ monooxygenases and SQases were  
 948 annotated as putative SMO gene clusters. (b) A phylogenetic tree demonstrating the diversity of  
 949 organisms possessing putative SMO gene clusters. The tree was constructed by pruning of the All-  
 950 Species Living Tree Project's 16s rRNA-based LTP release 132 ([https://www.arb-](https://www.arb-silva.de/projects/living-tree/)  
 951 [silva.de/projects/living-tree/](https://www.arb-silva.de/projects/living-tree/)).